Molecular Cell

Short Article

Stress-triggered hematopoietic stem cell proliferation relies on PrimPol-mediated repriming

Graphical abstract

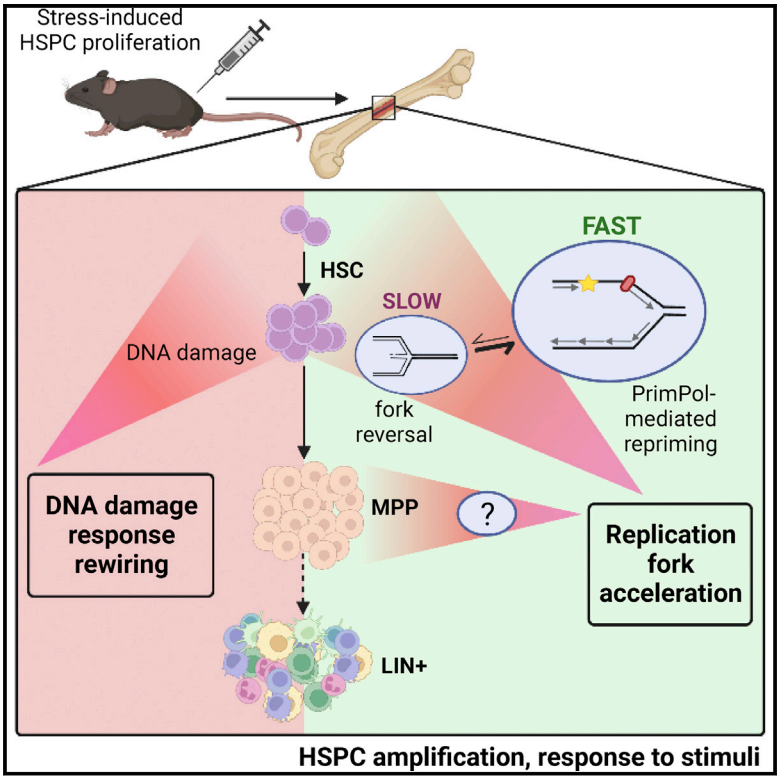

Highlights

- Proliferating HSCs incur ROS-independent breaks and rewire the DNA damage response
- HSPCs display accelerated replication fork progression upon induced proliferation
- Fast, discontinuous DNA synthesis in proliferating HSCs reflects Primpol engagement
- Primpol is required for sustained HSC proliferation and bone marrow reconstitution

Authors

Kurt Jacobs, Cyril Doerdelmann, Jana Krietsch, ..., Christine M. Eischen, Juan Mendez, Massimo Lopes

Correspondence

jmendez@cnio.es (J.M.), lopes@imcr.uzh.ch (M.L.)

In brief

Jacobs et al. found that DNA damage in stress-induced hematopoiesis confines to HSCs and triggers a rewired damage response. However, all hematopoietic stem and progenitor cells (HSPCs) undergoing induced proliferation accelerate replication fork progression, which—in HSCs—relies on Primpol-dependent repriming, promoting HSPC amplification and bone marrow reconstitution.

Jacobs et al., 2022, Molecular Cell *82*, 4176–4188
November 3, 2022
https://doi.org/10.1016/j.molcel.2022.09.009

CellPress

CellPress

Molecular Cell

Short Article

Stress-triggered hematopoietic stem cell proliferation relies on PrimPol-mediated repriming

Kurt Jacobs,[1,10] Cyril Doerdelmann,[1,10] Jana Krietsch,[1] Daniel González-Acosta,[1,3] Nicolas Mathis,[1] Saul Kushinsky,[2] Estrella Guarino,[3] Carmen Gómez-Escolar,[4] Dolores Martinez,[5] Jonas A. Schmid,[1] Peter J. Leary,[1,6] Raimundo Freire,[7,8,9] Almudena R. Ramiro,[4] Christine M. Eischen,[2] Juan Mendez,[3,*] and Massimo Lopes[1,11,*]

[1]Institute of Molecular Cancer Research, University of Zurich, Winterthurerstrasse 190, 8057 Zurich, Switzerland
[2]Department of Cancer Biology, Sidney Kimmel Cancer Center, Thomas Jefferson University, Philadelphia, PA, USA
[3]DNA Replication Group, Molecular Oncology Programme, Spanish National Cancer Research Centre (CNIO), Melchor Fernández Almagro 3, 28029 Madrid, Spain
[4]B Lymphocyte Biology Laboratory, Spanish National Center for Cardiovascular Research (CNIC), Melchor Fernández Almagro 3, 28029 Madrid, Spain
[5]Flow Cytometry Unit, Biotechnology Programme, Spanish National Cancer Research Centre (CNIO), Melchor Fernández Almagro 3, 28029 Madrid, Spain
[6]Functional Genomic Center Zurich, University of Zurich, Winterthurerstrasse 190, 8057 Zurich, Switzerland
[7]Unidad de Investigación, Hospital Universitario de Canarias, Tenerife, Spain
[8]Instituto de Tecnologías Biomédicas, Universidad de La Laguna, La Laguna, Spain
[9]Universidad Fernando Pessoa Canarias, Las Palmas de Gran Canaria, Spain
[10]These authors contributed equally
[11]Lead contact
*Correspondence: jmendez@cnio.es (J.M.), lopes@imcr.uzh.ch (M.L.)
https://doi.org/10.1016/j.molcel.2022.09.009

SUMMARY

Stem cell division is linked to tumorigenesis by yet-elusive mechanisms. The hematopoietic system reacts to stress by triggering hematopoietic stem and progenitor cell (HSPC) proliferation, which can be accompanied by chromosomal breakage in activated hematopoietic stem cells (HSCs). However, whether these lesions persist in their downstream progeny and induce a canonical DNA damage response (DDR) remains unclear. Inducing HSPC proliferation by simulated viral infection, we report that the associated DNA damage is restricted to HSCs and that proliferating HSCs rewire their DDR upon endogenous and clastogen-induced damage. Combining transcriptomics, single-cell and single-molecule assays on murine bone marrow cells, we found accelerated fork progression in stimulated HSPCs, reflecting engagement of PrimPol-dependent repriming, at the expense of replication fork reversal. Ultimately, competitive bone marrow transplantation revealed the requirement of PrimPol for efficient HSC amplification and bone marrow reconstitution. Hence, fine-tuning replication fork plasticity is essential to support stem cell functionality upon proliferation stimuli.

INTRODUCTION

The cumulative number of divisions in the stem cell population of a certain tissue is a strong indicator of the risk for cancerous transformation (Tomasetti et al., 2017), reflecting intrinsic chance of mutagenesis during DNA replication and external factors influencing replication fidelity (Wu et al., 2016). This marks DNA replication as a major contributor to genomic instability and emphasizes the impact of stem cell proliferation in tumorigenesis. The hematopoietic hierarchy forms a well-characterized stem cell-based system (Laurenti and Göttgens, 2018) and is ideal to study open questions on the interplay between proliferation, DNA replication, and genome instability. In the bone marrow, the long-term (LT-) hematopoietic stem cells (HSCs) form the most upstream, undifferentiated population, which gives rise to a chain of increasingly specialized downstream progenitors (Foudi et al., 2009; Wilson et al., 2008). The direct downstream population—the short-term (ST-) HSCs—is more proliferative and supports most of hematopoiesis together with the more differentiated multipotent progenitor (MPP) cells (Busch et al., 2015; Foudi et al., 2009; Sun et al., 2014). Altogether, HSCs and MPPs represent hematopoietic stem and progenitor cells (HSPCs). After further differentiation through more committed progenitor cells, the most downstream compartment consists of lineage-committed (Lin^+) cells which have no or very limited self-renewal capacity.

LT-HSCs must remain a functional population throughout life to support homeostasis. However, HSCs are reported to accumulate DNA damage during aging, which decreases their proliferation capacity (Flach et al., 2014) and contributes to the increased cancer risk with age (Rossi et al., 2007). Also, mutations occurring in the LT-HSCs are set to manifest over all downstream populations, potentially leading to a snowball effect (Rossi et al., 2008). The onset of disorders of the mammalian blood system, such as leukemia or Fanconi Anemia (FA), has so far been explained by progressive accumulation of mutations in HSPCs (Adams et al., 2015), highlighting the importance of DNA repair in the HSPC compartment. Upon ionizing radiation, LT-HSCs repair DNA double-stranded breaks (DSBs) predominantly through non-homologous end joining (NHEJ), an error-prone mechanism (Mohrin et al., 2010). Various other sources of DNA damage in HSCs have been reported, such as alcohol and aldehydes (Garaycoechea et al., 2012, 2018) or reactive oxygen species (ROS) (Tothova et al., 2007). However, the cross-talk between DNA replication dynamics and genome instability during homeostasis or stress-induced proliferation has not been thoroughly investigated.

LT-HSCs are predominantly quiescent, which is an important feature for maintaining a healthy and undamaged stem cell population (Orford and Scadden, 2008). Proliferation and differentiation in the hematopoietic system react rapidly to specific stimuli (Rieger and Schroeder, 2012). Active HSC proliferation can be induced by different stimuli, such as granulocyte colony-stimulating factor (Morrison et al., 1997), bacterial or viral infection (Baldridge et al., 2010; Essers et al., 2009), or bleeding (Cheshier et al., 2007). The interplay between proliferation and genome stability in HSCs is complex. On one hand, HSCs accumulate DNA damage during their mostly quiescent lifetime, which can be repaired after inducing proliferation (Beerman et al., 2014). On the other hand, HSC activation also induces DNA damage (Walter et al., 2015), and repetitive HSC activation can reduce HSC fitness over time, resembling accelerated aging (Essers et al., 2009; Matatall et al., 2016; Walter et al., 2015). How HSCs react to increased endogenous DNA damage during induced proliferation and whether induced proliferation modulates their response to exogenous DNA damage have remained elusive.

Overall, it is still unclear how exactly these proliferation bursts impact genome stability. A short "gap 1" (G1) phase has been recently linked in embryonic stem cells (ESCs) to a peculiar form of DNA replication stress (Ahuja et al., 2016) (Macheret and Halazonetis, 2015; Zeman and Cimprich, 2014). A strategy used by mammalian cells to cope with replication-associated problems is to pause the replication fork by actively converting it to a reversed replication fork, thereby allowing for lesion repair or stress release before restarting DNA synthesis (Berti et al., 2020; Zellweger et al., 2015). Fork stalling and remodeling upon stress are often coupled to controlled nucleolytic processing by specialized enzymes, which finally assists fork restart (Berti et al., 2020). An alternative strategy to allow rapid replication restart at obstacles is offered by the conserved primase PrimPol. Repriming DNA synthesis helps forks tolerating interstrand crosslinks and other lesions, counteracting fork reversal and promoting fast replication fork progression upon stress (Bai et al., 2020; García-Gómez et al., 2013; González-Acosta et al., 2021; Guilliam and Doherty, 2017; Kobayashi et al., 2016; Mourón et al., 2013; Piberger et al., 2020; Quinet et al., 2020). However, PrimPol-based replication restart entails discontinuous DNA synthesis, leaving gaps behind replication forks which require post-replicative repair (Bai et al., 2020; Mourón et al., 2013). PrimPol-independent mechanisms for replication fork acceleration have also been reported, and changes in replication fork speed have been recently linked to pathological conditions and specific developmental transitions (Bai et al., 2020; Hampp et al., 2016; Nakatani et al., 2022). Still, whether replication fork speed and plasticity are controlled during induced stem cell proliferation remains unknown.

Although DNA replication stress has been proposed as a possible cause for LT-HSC attrition and damage (Essers et al., 2009; Flach et al., 2014; Rossi et al., 2007; Walter et al., 2015), the underlying mechanisms have remained elusive. Also, most studies on genome stability in the hematopoietic system have been focused on HSCs, in light of their self-renewal capacities and their potential to originate hematological malignancies (Barabé et al., 2007; Huntly et al., 2004). However, downstream progenitor cells can also give rise to hematological cancers (Huntly et al., 2004; McCormack et al., 2010; Visvader, 2011), calling for a wider investigation on replication dynamics and associated genomic instability within the hematopoietic hierarchy. Here, we studied how the DNA replication process is affected when a simulated viral infection induces proliferation in the hematopoietic system. We report that induced proliferation in stem and progenitor cells is surprisingly accompanied by a drastic acceleration of replication fork progression. This altered fork dynamics reflect active suppression of replication fork reversal in favor of PrimPol-dependent repriming of DNA synthesis. Importantly, PrimPol is essential for sustained HSC proliferation and bone marrow reconstitution in competitive transplantation experiments, suggesting that a tight balance between reversal and repriming is crucial to support HSC proliferation and differentiation.

RESULTS

Stress-induced proliferation induces DNA breaks specifically in hematopoietic stem cells

First, we measured the proliferative status of hematopoietic cells *in vivo* in unperturbed conditions and upon a proliferation burst induced by a simulated infection. For this, we injected adult mice with polyinosinic:polycytidylic acid (pI:pC) to mimic a viral response, which was shown to induce proliferation in quiescent LT-HSCs (Essers et al., 2009). To label nascent DNA *in vivo*, we injected 5-ethynyl-2′-deoxyuridine (EdU) 45 min before euthanasia, which allowed for the identification of cycling cells and determination of the rate of DNA synthesis. LT-HSCs, ST-HSCs, MPPs (MPP4) and Lin^+ cells were freshly isolated based on a well-established combination of cell surface markers (Adolfsson et al., 2001; Boyer et al., 2019; Kiel et al., 2005; Mayle et al., 2013; Yang et al., 2005) (Figure 1A; see Figure S1A for surface marker combination and gating strategy). As expected based on previous work (Essers et al., 2009), both HSC populations increased their S-phase fraction already 12h post injection, and this effect reached a maximum at 48h, which was selected

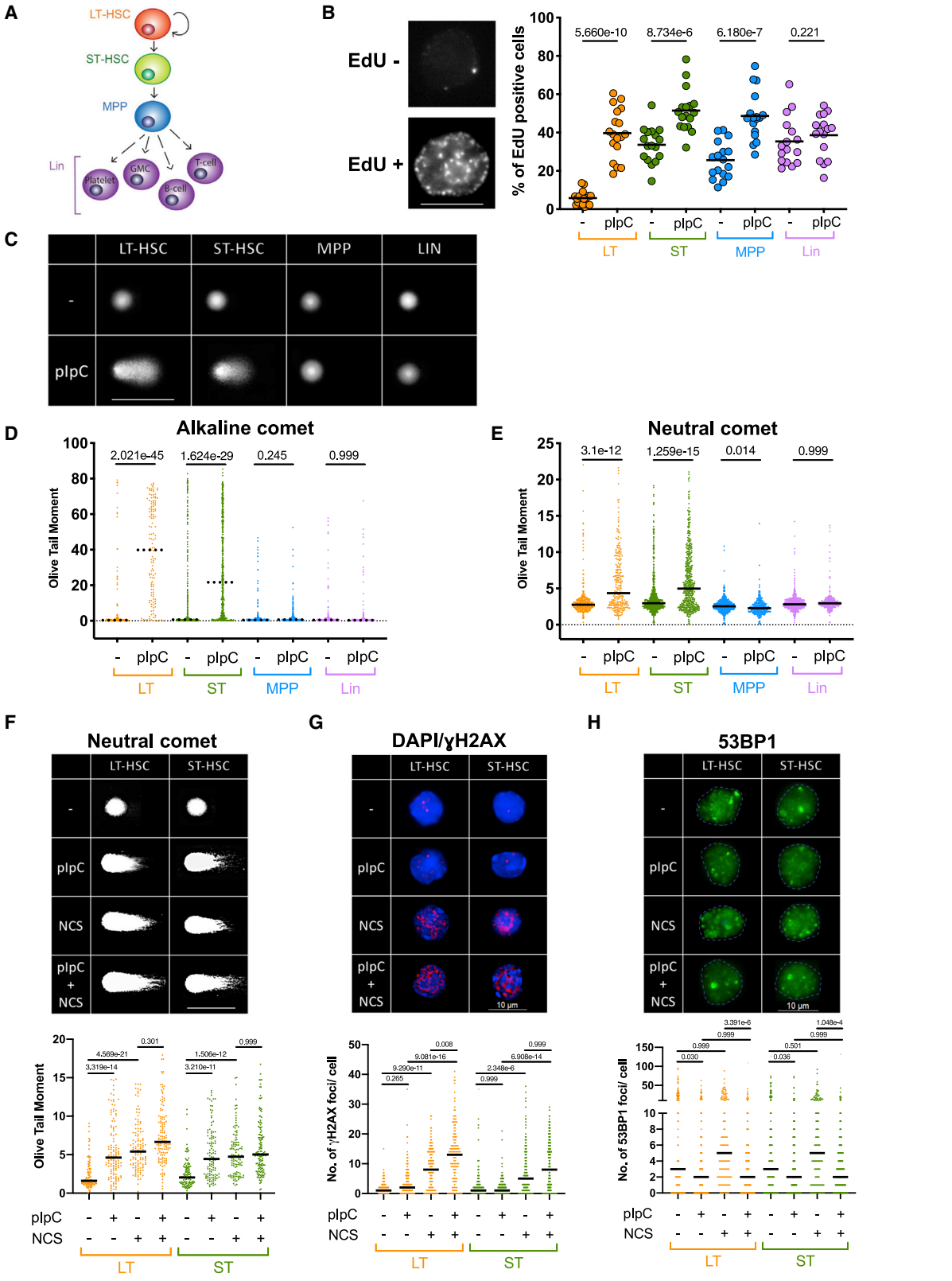

(legend on next page)

for further experiments (Figure S1B). The proliferation burst was particularly evident in normally quiescent LT-HSCs and extended to MPPs, while the terminally differentiated Lin$^+$ cells were unaffected (Figure 1B). Both interferon α (IFNα) stimulation *in vivo*, as well as short-term *in vitro* culture—previously shown to induce HSC proliferation (Essers et al., 2009; Walter et al., 2015)—yielded similar effects (Figure S1C), indicating that *in vivo* pI:pC treatment recapitulates established conditions of stress-induced proliferation. Using the alkaline comet assay, which detects both single-strand breaks (SSBs) and double-strand breaks (DSBs), we determined that induction of proliferation is accompanied by a strong increase of DNA breaks in LT-HSCs (Figures 1C, 1D, and S2A), as previously reported (Walter et al., 2015). Extending this analysis to other HSPC subpopulations, ST-HSCs also showed a sharp increase in DNA breakage. Conversely, MPPs displayed a similar cell cycle induction, but no increase in DNA damage (Figures 1B–1D and S2A). Using the neutral comet assay to specifically measure DSBs, we found these to also be exclusively induced in the HSC compartment (Figures 1E and S2B). Break accumulation seemed to occur specifically in a fraction of HSCs, while the rest retained basal levels of DNA breakage (Figures 1D and 1E), possibly reflecting a differential response to proliferation stimuli or different biological HSC subpopulations in the bone marrow (Christodoulou et al., 2020). Although the degree of damage induction varied, similar effects could be induced by *in vivo* IFNα stimulation and *in vitro* culturing (Figures S2C and S2D). Overall, although all tested progenitor cell types react to the stimuli by reaching comparable proliferation levels, only a fraction of LT- and ST-HSCs incur DNA damage.

Differential DNA damage response in hyper-proliferating hematopoietic cells

Proliferation-induced DNA breaks in LT-HSCs were originally linked to ROS caused by the activated metabolic state of the cells (Walter et al., 2015). We confirmed the occurrence of ROS-induced 8-oxoguanine (8oxoG) upon pI:pC stimulation by taking advantage of *in vitro* treatments with the specialized glycosylase OGG1 (Smith et al., 2006). Although a 14-day pre-treatment of the mice with the anti-oxidant N-acetylcysteine successfully prevented 8oxoG-associated (i.e., OGG1-sensitive) DNA damage (Figure S2E), a significant portion of the DNA breaks was still detectable following pI:pC stimulation (Figures S2F-S2G), suggesting that ROS only partially contributes to DNA damage accumulation in proliferating HSCs. Stress-induced hematopoiesis is associated with drastic acceleration of sequential cell cycles in otherwise quiescent LT-HSCs, implying short gap phases between consecutive S-phases. In constitutively proliferating ESCs, this scenario was linked to DNA replication stress and DNA damage, which can be relieved by prolonging the G1-phase with cyclin-dependent kinase (CDK) or CDC7-DBF4 kinase (DDK) inhibitors (Ahuja et al., 2016). However, *in vivo* treatment with Palbociclib (Cdk4/6 inhibitor) induced a transient delay in S-phase onset (5h), but failed to reduce DNA damage upon S phase re-entry (15h) (Figures S2H and S2I). Thus, differently from ESCs, gap phase length does not appear to significantly contribute to DNA damage induction in HSCs.

Although the source of the observed HSC-specific DNA breakage remains unclear, we investigated whether proliferation-associated DNA damage could activate a canonical DDR by comparing and combining *in vivo* pI:pC treatment with *in vitro* treatment with neocarcinostatin (NCS), a well-characterized clastogen. Neutral comet assays revealed that pI:pC injection in mice induces DSBs in both LT- and ST-HSCs at levels comparable to NCS (Figure 1F; Figure S3A). Whilst NCS-induced breaks expectedly activated the canonical DDR marker γH2AX in steady-state HSCs (Mohrin et al., 2010), to our surprise no significant increase in γH2AX foci count or intensity in HSCs was associated with pI:pC-induced damage (Figures 1G, S3B, and S3C). We then looked at 53BP1 recruitment to DSB foci as established readout of canonical DDR. After validating the staining conditions in 53BP1-knockout (KO) mouse embryonic fibroblasts (MEFs) (Figure S3D and S3E), we observed the expected increase in 53BP1 foci upon NCS treatment in steady-state HSCs (Figure 1H; Figure S3F) (Mohrin et al., 2010). Remarkably, despite the induced DSBs (Figure 1F), *in vivo* pI:pC treatment did not induce this response, and even prevented NCS-induced 53BP1 foci in both LT- and ST-HSCs (Figures 1H and S3F).

Figure 1. Activated HSCs specifically accumulate DNA damage and display a non-canonical DDR

(A) Schematic lineage tree of the hematopoietic stem, progenitor, and differentiated cell types used. Long-term (LT), short-term (ST), multipotent progenitor (MPP/MPP4), granulocyte/macrophage (GM).

(B) Representative staining of an EdU-positive and -negative cell (left, scalebar = 8μm) and EdU positive cells in percent (right) as quantified by quantitative image-based microscopy (QIBC), 48h after injection of pI:pC compared to untreated (−). To measure replication status *in vivo,* EdU was injected 45 min before sacrifice. Medians of 18 experiments are plotted as dots. Lines show averages.

(C) Representative images of an alkaline comet experiment conducted on freshly isolated subpopulations from untreated (upper row) and pI:pC-treated (lower row) mice. Scalebar = 100μm.

(D) Olive tail moment (OTM) values of a representative alkaline comet assay, conducted as in (C). A minimum of 100 cells was scored per sample. Dotted line marks the median. See Figure S2A for compiled repetitions.

(E) OTM of a representative neutral comet assay, 48h after injection of pI:pC compared to untreated (−) conditions. A minimum of 100 cells was scored per sample. Black line marks the median. See Figure S2B for compiled repetitions.

(F) Representative images and OTM of a neutral comet experiment. Scalebar = 125μm.

(G) Representative images and foci counts of a γH2AX immunofluorescence staining; 4′,6-diamidino-2-phenylindole (DAPI) is displayed to identify γH2AX-negative cells. Scalebar = 10μm.

(H) Representative images and foci counts of a 53BP1 immunofluorescence staining. Scalebar = 10μm.

(F–H) LT- and ST-HSCs were isolated 48h after pI:pC injection and optionally subjected to Neocarzinostatin (NCS, 1h 5 μg/ml) prior to comet/IF analysis. A minimum of 100 cells per sample was scored. Black line marks the median. Comet and IF experiments were performed in parallel on the same batch of freshly isolated and treated HSCs. See Figures S3A-S3C and S3F for compiled repetitions.

(B) Welch's t-test, (D–H) Kruskal-Wallis test. Indicated comparisons show numerical p values. See STAR methods for the number of animals per group.

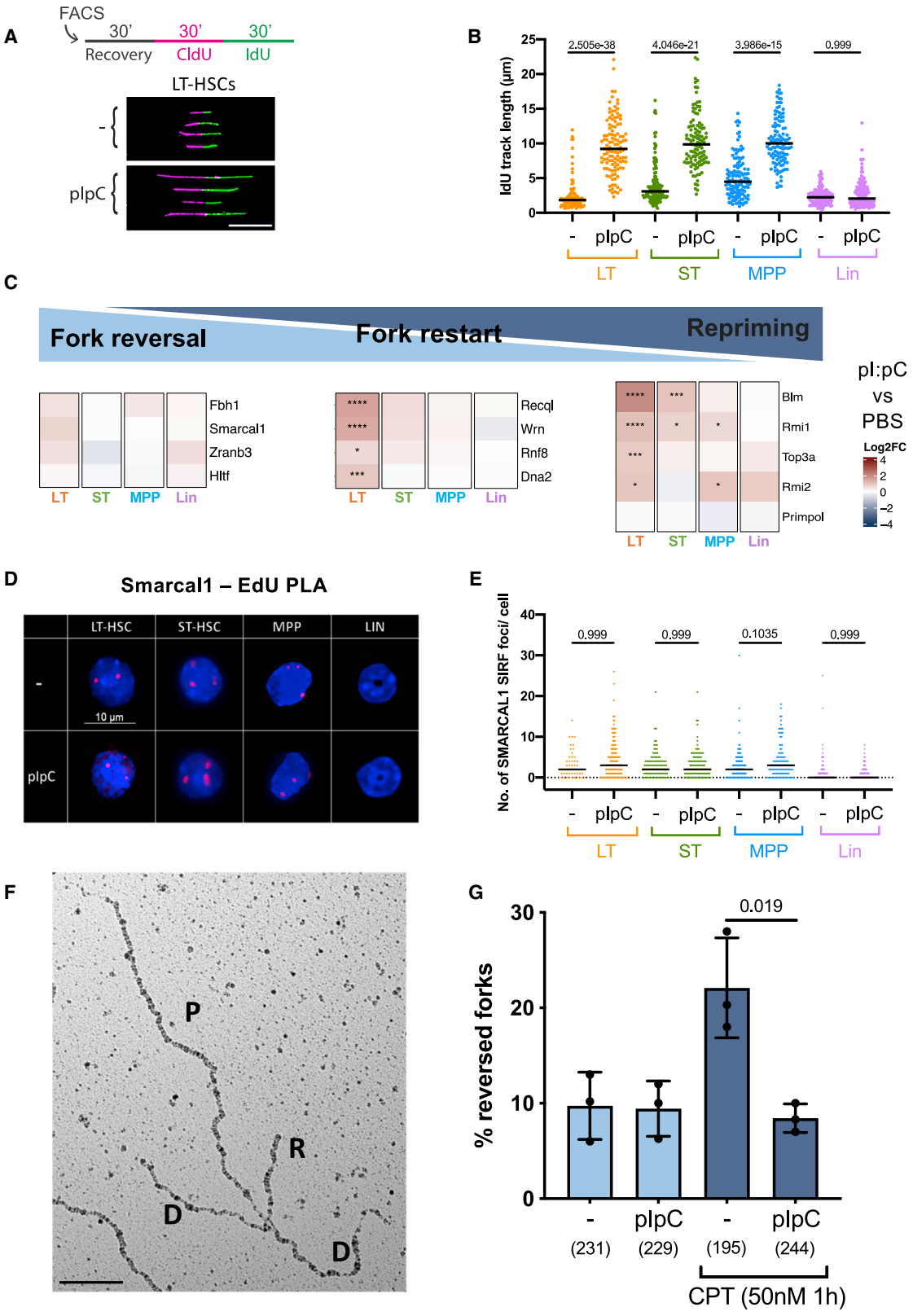

(legend on next page)

In order to investigate potential changes in gene expression underlying the observed modulation of the DDR, we conducted RNA-sequencing on three biological replicates of control (PBS) and pI:pC-treated mice. Unsupervised principal-component analysis showed that LT- and ST-HSCs cluster close together during unperturbed conditions but react differentially upon pI:pC stimulation (Figure S3G). Numerous genes involved in signaling DNA damage and replication stress were markedly induced in LT-HSCs and maintained at high levels in downstream HSPCs, supporting DDR activation in these conditions (Figures S3H and S4). Similarly, and in keeping with previous findings upon HSC culturing (Beerman et al., 2014), the vast majority of homologous recombination (HR) factors were also upregulated in HSCs by *in vivo* pI:pC treatment (Figures S3H and S4). Conversely, only a subset of NHEJ factors were upregulated in these conditions, and crucial factors of this pathway—e.g., Xrcc4 and 53BP1 (Trp53bp) itself—were significantly downregulated (Figures S3H and S4). These gene expression data provide an explanation for the surprising absence of 53BP1 foci upon DNA damage in proliferating HSCs. Moreover, these results suggest that, upon pI:pC-induced proliferation, HSCs rewire the canonical DDR and are likely to promote error-free DNA repair and tolerate proliferation-associated DNA damage.

Replication fork acceleration upon induced hematopoietic stem cell proliferation

In the attempt to further investigate genome stability and DDR modulation in the activated bone marrow, we then analyzed whether and how DNA replication dynamics is affected during stress-triggered HSPC hyperproliferation. In ESCs that constitutively proliferate or in somatic cells that experience oncogenic activation, DNA replication forks were shown to slow down or stall via active replication fork remodeling (Ahuja et al., 2016; Berti et al., 2020; Cortez, 2019; Neelsen et al., 2013). Freshly isolated HSPCs from mice that were or were not (controls) injected with pI:pC were pulse-labelled with nucleotide analogues and analyzed for replicated track length on spread DNA fibers, in order to measure replication fork speed at single-molecule level (Figure 2A). Surprisingly, pI:pC-induced HSPC proliferation led to a marked and reproducible acceleration of replication fork progression in all HSPC populations (HSCs and MPPs), while fork speed in Lin^+ cells was not affected (Figures 2B and S5A–S5B). Increased track length does not reflect increased fork density and fusions, as pI:pC did not detectably affect origin firing or termination events in our experimental conditions (Figure S5C). Replication fork acceleration was observed to various extents using different proliferation stimuli (Figure S5D) and is thus inherently linked to stress-induced HSPC proliferation.

We next interrogated our RNA-sequencing data (Figures S3G–S3H) to reveal possible changes underlying the observed change in replication dynamics. This analysis expectedly revealed numerous genes encoding for replication initiation factors that were induced by pI:pC treatment in different HSPC populations, reflecting the observed increase in S-phase cell fraction (Figures 1B and S5E). However, while considering specialized factors involved in the replication stress response, we noticed that mediators of replication fork reversal—such as the DNA translocases Smarcal1 and Zranb3 (Betous et al., 2013; Kolinjivadi et al., 2017; Vujanovic et al., 2017)—are upregulated only mildly (if at all) in HSCs and MPPs from pI:pC-injected mice (Figure 2C). Conversely, factors limiting or resolving reversed forks—e.g., the RecQ-homologues RecQ1 (Recql) and Wrn helicases (Berti et al., 2013, 2020; Thangavel et al., 2015; Zellweger et al., 2015)—are significantly upregulated upon pI:pC, particularly in LT-HSC (Figure 2C).

These observations suggested to us that—particularly in HSCs—pI:pC-induced proliferation is accompanied by changes in replisome composition, which may counteract fork reversal. To directly test the functional contribution of fork reversal to fork speed and genome integrity following pI:pC stimulation, we performed DNA fiber and comet assays with HSPCs from mice lacking Smarcal1 or Zranb3, two key fork-reversal factors in cultured cells (Kolinjivadi et al., 2017; Vujanovic et al., 2017). These mice are resistant to hematological malignancy development upon ionizing radiation damage of HSCs (Puccetti et al., 2017) or c-Myc overexpression in B-cells (Puccetti et al., 2019), likely reflecting replication fork collapse and subsequent apoptosis of the cells that cannot mitigate the replication stress.

Figure 2. Upon stress-induced proliferation, HSPCs display accelerated fork progression and counteract fork reversal

(A) Schematic overview (top) and compiled image of cropped, representative DNA fiber tracks on black background (bottom) of the DNA fiber spreading procedure applied to LT-HSCs from unstimulated (–) or pI:pC-treated mice. Freshly isolated cell populations were allowed to recover for 30 min before nucleotide analog-labelling as depicted. CldU/IdU-tracks were immunostained and displayed in magenta and green, respectively. 5-iodo-2'-deoxyuridine (IdU) track length of double-labelled tracks (ongoing forks) were measured to assess replication fork speed. Scalebar = 10μm.

(B) IdU track length of one biological replicate, 48h after optional pI:pC treatment. A minimum of 100 fibers was scored per sample. Black line marks the median. See Figure S5B for compiled repetitions.

(C) Tile map of the log2 fold change and significance of pI:pC versus PBS for each cell line as calculated from differential expression using DESeq2. Color denotes log2 fold change where red (positive) is higher in pI:pC and blue (negative) is higher in PBS. Asterisks denote FDR-corrected p values: **** = $p < 0.0001$; *** = $p < 0.001$; and; * = $p < 0.05$. Genes were clustered by log2 fold change using Ward's hierarchical clustering.

(D) Representative images of SMARCAL1 "*in situ* analysis of protein interactions at DNA replication forks" (SIRF) foci (red) over DAPI staining. Scalebar = 10μm.

(E) Foci count of a representative SMARCAL1 SIRF replicate, 48h after optional injection of pI:pC. Black bar indicates median. See Figure S5I for compiled repetitions.

(F) Representative EM image of a reversed replication fork obtained from freshly isolated mouse bone marrow. P, parental strand; D, daughter strand; R, regressed arm.

(G) Frequency of reversed forks in total bone marrow cells isolated from mice, optionally treated *in vivo* with pI:pC and *ex vivo* with CPT (50nM, 1h), prior to psoralen-crosslinking followed by DNA extraction. Data from 3 biological replicates are depicted as mean ± SEM. Brackets = total number of replication intermediates analyzed per sample.

(B and E) Kruskal-Wallis test, (G) Welch's t-test. Indicated comparisons show numerical p values. See STAR methods for the number of animals per experimental group.

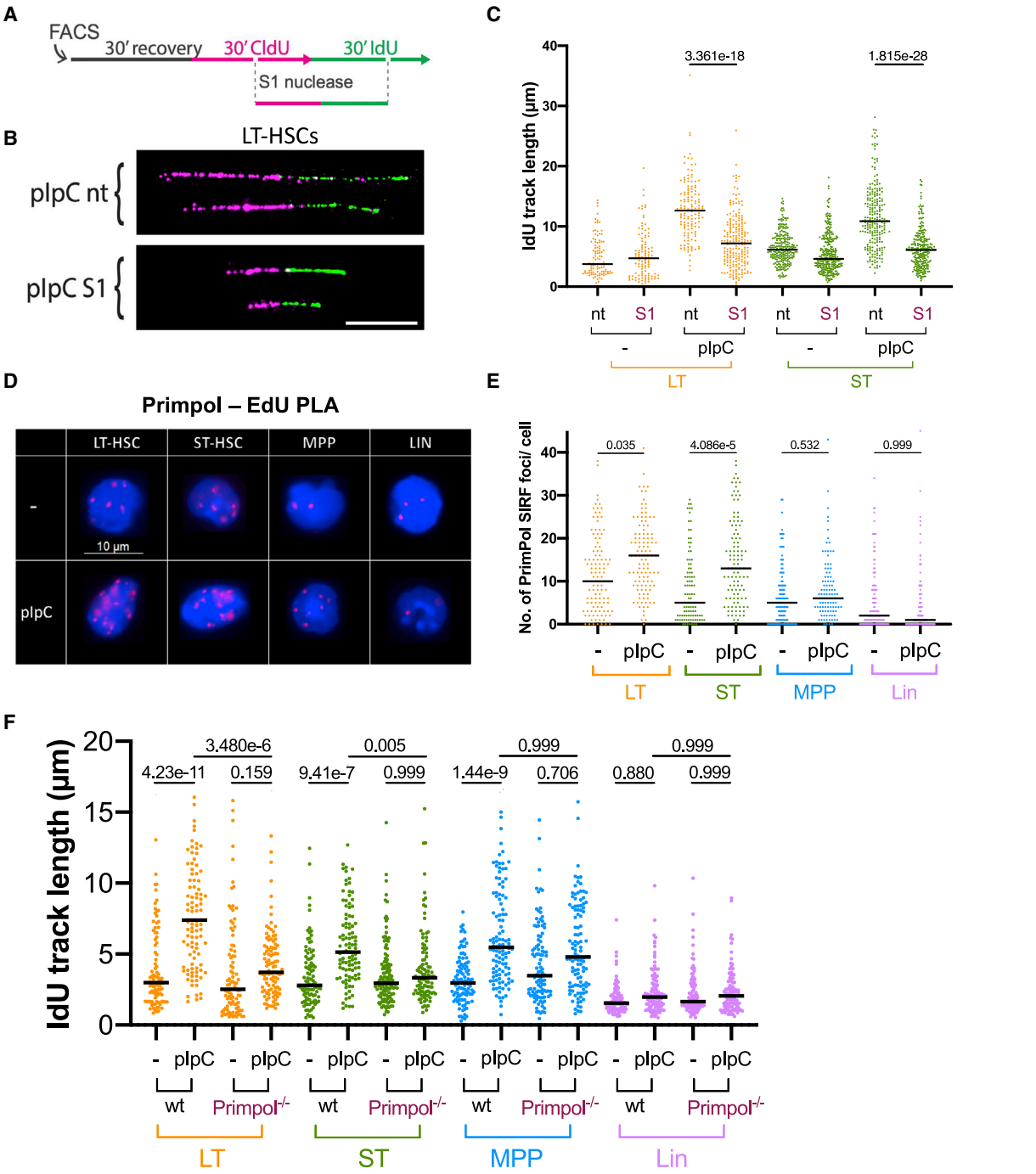

Figure 3. Proliferating HSCs display fast, discontinuous DNA synthesis mediated by PrimPol

(A) Schematic display of the DNA fiber spreading assay coupled with ssDNA-specific S1 nuclease treatment for the detection of ssDNA gaps/discontinuities on ongoing forks. Isolated cells were allowed to recover 30 min and then incubated with nucleotide-analogs, followed by optional treatment with the S1 nuclease. CldU/IdU-tracks were immunostained and displayed in magenta and green, respectively; IdU track length of double-labelled tracks were measured to assess replication fork speed.

(B) Compiled image of cropped, representative DNA fiber tracks on black background from unstimulated (–) or pI:pC-treated LT-HSCs. White scalebar = 10μm.

(C) Representative biological replicate of IdU track length in unstimulated (–) cells or 48h after pI:pC treatment with optional S1 nuclease digestion. Black bars represent medians. A minimum of 100 tracks was measured per sample. See Figure S6A for compiled repetitions.

(D) Representative images of PrimPol SIRF foci (red) over DAPI staining. Scalebar = 10μm.

(legend continued on next page)

However, replication fork acceleration and DNA damage induction in the *Smarcal1*-or *Zranb3*-deficient HSCs detected upon pI:pC stimulation closely resembled what was observed in wild-type (WT) controls (Figures S5F and S5G). While not excluding a possible functional relevance for fork reversal for the replenishment of the HSPC compartment upon prolonged or repeated stress (Puccetti et al., 2017), these data demonstrate that efficient fork reversal mediated by Smarcal1 or Zranb3 is dispensable for the observed accelerated fork speed and the accumulated DNA damage upon acute pI:pC stimulation. In agreement with this, proximity ligation assays (PLA) of proven specificity (Figures S5H) revealed that Smarcal1 engagement at EdU is minimal in steady-state HSPCs and is not induced upon pI:pC-induced proliferation (Figures 2D–2E and S5I).

Visualization of individual replication intermediates by electron microscopy (EM) is currently the method of choice to directly quantify replication fork reversal (Zellweger and Lopes, 2017). Despite numerous attempts, it proved technically impossible in our hands to optimize an EM protocol to study replication forks in the HSPC populations due to their extremely low cell numbers and the small fraction of replicating cells. Nonetheless, we chose to perform EM-based replication-fork analysis in total bone marrow cells isolated from mice that were either treated or not treated with pI:pC. As previously shown in cultured cell lines (Chaudhuri et al., 2012; Zellweger et al., 2015), freshly isolated bone marrow cells were capable of drastically increasing the fraction of reversed forks upon mild *ex vivo* treatment with the Topoisomerase I inhibitor camptothecin (CPT) (Figures 2F–2G). Strikingly, the fork-reversal rate was not changed by CPT treatment if bone marrow cells were isolated after *in vivo* pI:pC stimulation (Figure 2G). Altogether, these data suggest that—while rapidly proliferating—pI:pC-stimulated bone marrow cells suppress fork reversal, preferring alternative replication mechanisms that accelerate replication fork progression.

PrimPol mediates fast, discontinuous DNA synthesis in proliferating hematopoietic stem cells

PrimPol-based repriming can be used by cancer cells to bypass genotoxic lesions (Mourón et al., 2013), promoting accelerated fork progression upon mild genotoxic stress (Bai et al., 2020; Berti et al., 2020; Quinet et al., 2020). Although PrimPol expression itself is not altered upon pI:pC treatment, several members of the PrimPol-interacting BTR-complex (Blm, Rmi1, Rmi2, and Top3a) (González-Acosta et al., 2021) are upregulated in HSPCs (Figure 2C), possibly hinting at repriming as molecular determinant of accelerated fork progression.

PrimPol-dependent repriming produces a discontinuous daughter strand, leaving single-stranded DNA (ssDNA) gaps behind the moving fork. Those gaps can be detected and processed by the ssDNA-specific S1 endonuclease while performing the DNA fiber assay (Quinet et al., 2017), resulting in shortened DNA fiber tracks (Figures 3A and 3B). We determined that DNA fibers from LT-HSCs and ST-HSCs of pI:pC injected mice were indeed sensitive to S1 nuclease digestion (Figures 3C and S6A). Accordingly, after ensuring the specificity of our antibody and of the assay (Figure S6B–S6D), PLA revealed a significant increase in PrimPol recruitment to EdU upon pI:pC treatment in HSCs but not in MPPs (Figures 3D–3E and S6E). Furthermore, applying the DNA fiber assay to HSPC from *Primpol*$^{-/-}$ mice, we found that pI:pC-induced fork acceleration in both LT- and ST-HSCs is largely Primpol dependent, while this was not the case for MPPs (Figures 3F and S6F). Thus, PrimPol mediates pI:pC-induced fork acceleration in both HSC subpopulations, while it is dispensable for fork acceleration in MPPs. Overall these data suggest that PrimPol-mediated fast and discontinuous replication is activated to enable the rapid response to pI:pC-induced proliferation.

To test if PrimPol-mediated repriming is required for induced proliferation and is functionally linked to the associated chromosomal breakage in hematopoietic cells, we performed neutral comet assays on HSPCs from *Primpol*$^{-/-}$ mice and WT littermates 48h after pI:pC treatment. In *Primpol*$^{-/-}$ mice, we detected normal induction of HSC proliferation and no significant difference in DSB generation (Figures S7A and S7B), supporting the idea that most of the observed DSBs are not a direct consequence of repriming or fast fork progression, at least at the time point selected for our analysis (48h after pI:pC injection).

FA factors are crucial for HSC genome stability and survival during chronically induced proliferation (Walter et al., 2015). We thus set out to investigate the contribution of the FA pathway to the stress-induced DSBs and changes in replication dynamics. At the time point selected for our analysis, mice deficient for *Fanca*—a member of the FA core complex and the most commonly mutated gene in FA patients (Taniguchi and D'Andrea, 2006)—displayed normal induction of HSC proliferation and no significant difference in proliferation-associated DSB induction (Figures S7C–S7D). Moreover, HSCs from *Fanca*$^{-/-}$ mice were still perfectly able to accelerate replication fork progression and to accumulate discontinuities on the daughter strands upon pI:pC stimulation (Figures S7E–S7F). This result identifies PrimPol-mediated fork acceleration as an independent mechanism supporting HSC proliferation, distinct from the contribution of the FA pathway.

Hematopoietic stem cells rely on Primpol for proper bone marrow reconstitution

In line with the data described above (Figures S7A and S7B), we did not observe any significant difference in the absolute numbers of bone marrow HSCs between WT and *Primpol*$^{-/-}$ mice either before or 48h after pI:pC injection (Figure S8A). While these data exclude a strict requirement for PrimPol for proliferation *per se* in the initial burst of HSC expansion, they leave room for PrimPol-mediated repriming sustaining long-term HSC proliferation and functionality. To address this possibility,

(E) Foci counts of a representative PrimPol SIRF replicate, 48h after injection of pI:pC compared to untreated (–) conditions. Black bar indicates median. See S6E for compiled repetitions.

(F) IdU track length of a biological replicate in unstimulated (–) cells or 48h after pI:pC treatment in wt or *Primpol*$^{-/-}$ mice. Black line marks the median. A minimum of 100 tracks per sample was measured. See Figure S6F for compiled repetitions.

(C, E, and F) Kruskal-Wallis test. Indicated comparisons show numerical p values. See STAR methods for the number of animals per experimental group.

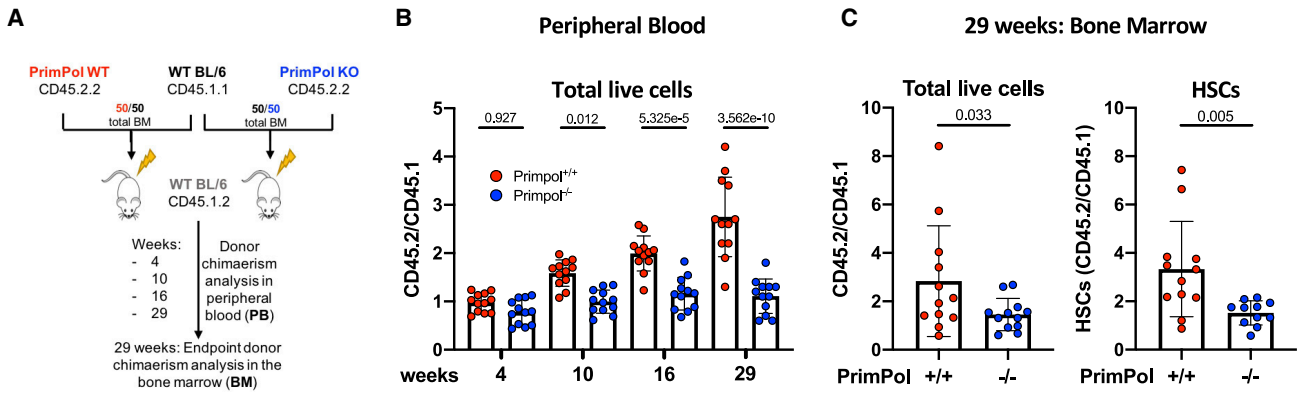

Figure 4. Efficient bone marrow reconstitution upon stress requires PrimPol

(A) Schematic of the competitive transplantation assay performed to compare bone marrow reconstitution ability of freshly isolated PrimPol wt versus *Primpol*$^{-/-}$ donor cells in lethally irradiated recipient mice. Two donor pools with varying surface marker isoforms—CD45.1.1 WT "black 6" (BL/6) cells and CD45.2.2 either *Primpol* wt or *Primpol*$^{-/-}$ cells—were prepared to each make up for 50% of the injected donor material. To assess donor chimerism, ratios of peripheral blood (PB) cells carrying the respective CD45 isoforms were determined at 4, 10, 16, and 29 weeks post transplantation. At 29 weeks, mice were sacrificed, femurs were harvested, and donor chimerism was assessed as above for total bone marrow or hematopoietic stem cells.

(B) Donor chimerism assessed as isoform ratios of total live PB cells at the indicated time post transplantation. Ratios from 12 recipient mice per group are plotted as dots.

(C) Donor chimerism displayed as CD45 isoform ratios of total live bone marrow cells (left) or HSCs (right) 29 weeks after transplantation. Ratios from 12 (+/+) and 11 (−/−) recipient mice per group are plotted as dots.

(B) One-way ANOVA.

(C) Welch's t-test. Indicated comparisons show numerical p values. See also Figure S8.

freshly isolated bone marrow cells expressing the CD45.2.2 surface marker from WT or *Primpol*$^{-/-}$ deficient mice were transplanted into lethally irradiated recipient mice expressing the CD45.1.2 marker in competition (1:1 ratio) with WT bone marrow cells that express CD45.1.1 (Figures 4A and S8B). Marked defects in competitive bone marrow reconstitution were observed for *Primpol*$^{-/-}$-deficient CD45.2-derived cells, as evidenced in peripheral blood analyses. Reduced CD45.2/CD45.1 ratios from *Primpol*$^{-/-}$ compared to WT donors were observed in live peripheral blood cells as early as 4 weeks after transplantations (Figure 4B). Defective competitive reconstitution of cells derived from *Primpol*$^{-/-}$ donors was progressively more marked at later time points and was clearly detectable in all examined differentiated subpopulations in the peripheral blood (Figures 4B and S8C–S8D). At the endpoint of the experiment (29 weeks after bone marrow transplantation [BMT]), bone marrow analyses confirmed significantly reduced competitive reconstitution of *Primpol*$^{-/-}$ transplanted cells compared to WT counterparts, as detected by CD45.2/CD45.1 ratio in total living cells and HSCs (Figures 4C and S8E). These data clearly establish PrimPol as key factor for HSC fitness and functionality upon induced proliferation and engraftment.

DISCUSSION

Our analysis of DNA replication dynamics and genome integrity reveals that HSPCs undergoing proliferation bursts modify their replication mode toward faster and discontinuous DNA synthesis. We propose that these molecular adaptations are necessary to cope with the need for extremely rapid proliferation combined with transcriptional bursts that drive differentiation into different lineages. Albeit possibly challenging for genome integrity, these responses are required to promptly respond to infections and other types of stress requiring rapid generation of new blood cells. These surprising data extend previous observations in constitutively proliferating ESCs, showing massive accumulation of ssDNA gaps, which are tolerated during cell division and do not activate DNA damage checkpoints (Ahuja et al., 2016; Aladjem et al., 1998). Also, the suppression in ESCs of canonical genome maintenance mechanisms present in somatic cells can drastically increase mutational load in blastomeres (Jacobs et al., 2017), as rapid mass expansion is crucial for embryo survival, and apoptosis helps eliminate excessively damaged cells (Kiessling, 2010; Stambrook and Tichy, 2010; Wong et al., 2010). Similarly, differentiated blood cells—rapidly produced during proliferation bursts—are mostly short lived, making their potential genomic instability an acceptable price to pay to allow rapid tissue plasticity in response to stimuli. In this respect, we note that more committed progenitors (i.e., MPPs) share with HSCs a fast replication mode, which, however, is neither PrimPol dependent nor associated with chromosomal breakage. Intriguingly, an alternative PrimPol-independent mode of replication-fork acceleration was recently reported upon a specific genetic perturbation of fork reversal and requires the error-prone translesion polymerase Rev1 (Bai et al., 2020). It will be important to assess whether—once committed toward differentiation—stem and progenitor cells favor an increased mutational load over a challenge to chromosome integrity while maintaining sustained proliferation.

Our data support the physiological relevance of maintaining a proper equilibrium between different DNA damage tolerance pathways for adult stem cell proliferation, extending recent findings on the modulation of fork progression in specific physio-pathological conditions (Hampp et al., 2016; Maya-Mendoza et al., 2018;

Nakatani et al., 2022). The equilibrium between fork reversal and repriming was recently proposed to modulate the response to genotoxic chemotherapeutic treatments in cancer cells (Bai et al., 2020; Quinet et al., 2020). We now report that the same balance appears crucial for the plastic equilibrium between quiescence and stimuli-induced proliferation, as observed in hematopoiesis. Although our data show active suppression of fork reversal during acute pI:pC-induced proliferation, mice rely on Smarcal1 fork reversal activity to cope with DNA-damage-induced HSPC attrition to fully reconstitute the hematopoietic system and to undergo damage-induced lymphomagenesis (Puccetti et al., 2017). Additionally, both Smarcal1 and Zranb3 DNA translocases are essential for mitigating replication stress in primary B cells when chronically stimulated *in vivo* by the c-Myc oncogene (Puccetti et al., 2019). Overall, rather than being mutually exclusive, fork reversal and repriming likely require fine-tuning in time and space in order for mice to efficiently respond to different insults in the hematopoietic system. Understanding the mechanisms by which HSPCs control this equilibrium in the frame of induced proliferation and differentiation will be a fascinating challenge for the future. Optimizing EM protocols as well as other single-cell and single-molecule assays for extremely low cell numbers will be instrumental to uncover frequency and relevance of fork remodeling in HSPC populations in response to different proliferation stimuli.

In line with previous evidence (Walter et al., 2015), our data reveal a marked accumulation of DSBs in proliferating HSCs. We now show that these breaks do not specifically reflect accumulated oxidative stress or accelerated fork progression. Moreover, DSBs are restricted to HSCs and not detectable in multipotent progenitors which are immediately downstream in the differentiation cascade, suggesting that efficient DNA repair—or elimination of damaged cells—is coupled to the earliest steps of HSC differentiation. DSB repair was previously reported to be boosted and rewired when HSCs are induced to proliferate by transient culturing, showing a marked induction of HR versus NHEJ (Beerman et al., 2014). In line with these findings, we now report that multiple DDR genes—mostly driving HR—are promptly induced upon pI:pC treatment. Conversely, several essential NHEJ factors (53BP1, Rif1, Xrcc4, DNA-PK) are only marginally induced or even repressed upon pI:pC. Accordingly, 53BP1 is not efficiently recruited to sites of DNA damage in proliferating HSCs, even when exogenous DNA damage is inflicted on top of proliferation-associated DSBs. This important evidence suggests that—besides replication fork plasticity—DNA repair and DNA damage signaling also need to be properly tuned in HSCs to maintain genome integrity and sustain proliferation, likely entailing yet-elusive post-translational modifications of key DDR factors. Full mechanistic understanding of DNA-damage occurrence and repair in proliferating HSCs will also require time-resolved animal experiments and specialized methods to monitor DNA damage/repair within the intact bone marrow (Mun and Nombela-Arrieta, 2021) in order to possibly link DNA damage and/or repair to specific stem cell niches.

As suggested by our BMT results, a proper fine-tuning of replication fork plasticity may be required after prolonged proliferation to tolerate or repair accumulated DNA damage, thereby enabling the physiological expansion of bone marrow cells and the necessary supply of differentiated cells in the peripheral blood. It is yet unclear which source of endogenous damage requires this accurate tuning of DNA damage tolerance mechanisms in replication. Endogenous and alcohol-derived aldehydes represent a major potential source of genomic instability in HSCs, inducing endogenous inter-strand crosslinks (ICLs) that require FA factors for repair and replication tolerance (Garaycoechea et al., 2012, 2018; Langevin et al., 2011). Replication forks are also known to stall at endogenous sequences which are intrinsically difficult to replicate, often due to their propensity to form secondary structures (Follonier et al., 2013; Schmid et al., 2018). Alternatively, replication-fork plasticity may be required to accommodate endogenous transcription-replication conflicts. Such conflicts are likely exacerbated in the context of stress-induced stem cell proliferation, which entails transcriptional bursts during differentiation in blood lineages. Dealing with these unavoidable replication challenges by fine-tuning fork remodeling and repriming activities may be necessary to rapidly obtain a sufficient number of hematopoietic effector cells and properly respond to the stimulus.

Overall, our results shed light on the specific modulation of DNA-replication and DNA-damage responses that enable HSCs to address challenges to genome integrity associated with stress-induced proliferation and to reconstitute the full hematopoietic system from very few cells. In light of the tight–albeit elusive—link between stem cell division and tumorigenesis (Tomasetti et al., 2017), further molecular investigations into DNA replication during sustained stem cell proliferation are likely to illuminate key mechanistic aspects of tumorigenesis. Moreover, as leukemias most frequently originate from uncontrolled HSPC proliferation and are treated with genotoxic drugs that interfere with DNA replication (Vetrie et al., 2020), mechanistic insight into these processes may identify new vulnerabilities to exploit for improved chemotherapy of leukemic cells.

Limitations of the study

HSPCs used in this study were stimulated *in vivo* and analyzed for replication and DDR parameters shortly after isolation. Preserving the hematopoietic bone marrow niche and its architecture by avoiding the necessity of cell isolation will be instrumental to decipher the yet-unknown mechanistic details of DDR rewiring and replication fork plasticity in activated HSPCs.

STAR★METHODS

Detailed methods are provided in the online version of this paper and include the following:

- KEY RESOURCES TABLE
- RESOURCE AVAILABILITY
  - Lead contact
  - Materials availability
  - Data and code availability
- EXPERIMENTAL MODEL AND SUBJECT DETAILS
  - Mouse models
- METHOD DETAILS
  - Mouse manipulations and group sizes
  - Isolation of hematopoietic cell subsets
  - Immunostaining

- Quantitative image-based microscopy
- Proximity ligation assay
- Comet assay
- DNA fiber assay
- S1 nuclease fiber assay
- Transcriptome analysis
- EM analysis
- Primpol antibody generation
- Hematopoietic stem and progenitor cell counting
- Competitive bone marrow transplantation assays

● QUANTIFICATION AND STATISTICAL ANALYSIS

SUPPLEMENTAL INFORMATION

Supplemental information can be found online at https://doi.org/10.1016/j.molcel.2022.09.009.

ACKNOWLEDGMENTS

We are grateful to M. Manz for the assistance with the initial phase of this study. We thank S. Ursich, A. Quinet, S. Mur (CNIC), R. Heyard (Center for Reproducible Science, UZH), A.L. Pereira and C. Nombela-Arrieta (Hematology, USZ), M. Altmeyer (DMMD), the Functional Genomic Center Zurich, the Laboratory Animal Services Center, the Cytometry Facility, and the Center for Microscopy and Image Analysis of the University of Zurich for technical assistance and fruitful discussions. Work in the Lopes lab was supported by the ERC Consolidator Grant 617102 (ReStreCa) and the SNF grant 310030_189206. Work in the Mendez lab was supported by the Spanish Ministry of Science and Innovation (grants BFU2016-80402-R and PID2019-106707-RB, co-sponsored by ERDF funds from the EU). Work in the Eischen lab was supported by NIH/NCI grants R01CA226432 and P30CA056036 for supporting the Flow Cytometry and Lab Animals core facilities, by the Herbert A. Rosenthal endowed chair fund, and by a gift from the Seinfort family. Work in the Ramiro lab was supported by the Spanish Ministerio de Ciencia e Innovación (PID2019-106773RB-I00/ AEI / 10.13039/501100011033). R.F. was supported by the Spanish Agencia Estatal de Investigación (PID2019-109222RB-I00/AEI/10.13039/501100011033), co-sponsored by ERDF funds from the EU.

AUTHOR CONTRIBUTIONS

Conceptualization and methodology, K.J., C.D., J.K., J.M., and M.L. with assistance from C.M.E.; Investigation at UZH, Switzerland, K.J. and C.D. with assistance from J.K., D.G.-A., and N.M.; Investigation at CNIO, Spain, K.J. with assistance from D.G.-A. and J.M.; Investigation at TJU, USA, K.J. with assistance from S.K. and C.M.E.; Conceptualization and methodology BMT, J.M., A.R.R. with assistance from C.M.E. and S.K.; Investigation BMT, E.G., D.M., and C.G.-E.; Assistance with EM analysis, J.A.S.; RNA-seq analysis, P.J.L.; Resources, C.M.E., J.M., and R.F.; Funding acquisition and supervision, M.L.; Writing, reviewing, and editing, M.L. with assistance from J.K. and C.D. All authors read and provided feedback on the manuscript.

DECLARATION OF INTERESTS

The authors declare no competing interests.

Received: September 9, 2020
Revised: July 1, 2022
Accepted: September 8, 2022
Published: September 23, 2022

REFERENCES

Adams, P., Jasper, H., and Rudolph, K. (2015). Aging-Induced Stem Cell Mutations as Drivers for Disease and Cancer. Cell Stem Cell *16*, 601–612. https://doi.org/10.1016/j.stem.2015.05.002.

Adolfsson, J., Borge, O.J., Bryder, D., Theilgaard-Mönch, K., Åstrand-Grundström, I., Sitnicka, E., Sasaki, Y., and Jacobsen, S.E. (2001). Upregulation of Flt3 Expression within the Bone Marrow Lin−Sca1+c-kit+ Stem Cell Compartment Is Accompanied by Loss of Self-Renewal Capacity. Immunity *15*, 659–669. https://doi.org/10.1016/s1074-7613(01)00220-5.

Ahuja, A.K., Jodkowska, K., Teloni, F., Bizard, A.H., Zellweger, R., Herrador, R., Ortega, S., Hickson, I.D., Altmeyer, M., Mendez, J., and Lopes, M. (2016). A short G1 phase imposes constitutive replication stress and fork remodelling in mouse embryonic stem cells. Nat. Commun. *7*, 10660. https://doi.org/10.1038/ncomms10660.

Aladjem, M.I., Spike, B.T., Rodewald, L.W., Hope, T.J., Klemm, M., Jaenisch, R., and Wahl, G.M. (1998). ES cells do not activate p53-dependent stress responses and undergo p53-independent apoptosis in response to DNA damage. Curr. Biol. *8*, 145–155. https://doi.org/10.1016/s0960-9822(98)70061-2.

Bai, G., Kermi, C., Stoy, H., Schiltz, C.J., Bacal, J., Zaino, A.M., Hadden, M.K., Eichman, B.F., Lopes, M., and Cimprich, K.A. (2020). HLTF Promotes Fork Reversal, Limiting Replication Stress Resistance and Preventing Multiple Mechanisms of Unrestrained DNA Synthesis. Mol Cell *78*, 1237–1251.e7. https://doi.org/10.1016/j.molcel.2020.04.031.

Baldridge, M.T., King, K.Y., Boles, N.C., Weksberg, D.C., and Goodell, M.A. (2010). Quiescent hematopoietic stem cells are activated by IFN-γ in response to chronic infection. Nature *465*, 793–797. https://doi.org/10.1038/nature09135.

Barabé, F., Kennedy, J.A., Hope, K.J., and Dick, J.E. (2007). Modeling the Initiation and Progression of Human Acute Leukemia in Mice. Science *316*, 600–604. https://doi.org/10.1126/science.1139851.

Beerman, I., Seita, J., Inlay, M., Weissman, I., and Rossi, D. (2014). Quiescent hematopoietic stem cells accumulate DNA damage during aging that is repaired upon entry into cell cycle. Cell Stem Cell *15*, 37–50. https://doi.org/10.1016/j.stem.2014.04.016.

Berti, M., Ray Chaudhuri, A., Thangavel, S., Gomathinayagam, S., Kenig, S., Vujanovic, M., Odreman, F., Glatter, T., Graziano, S., Mendoza-Maldonado, R., et al. (2013). Human RECQ1 promotes restart of replication forks reversed by DNA topoisomerase I inhibition. Nat. Struct. Mol. Biol. *20*, 347–354. https://doi.org/10.1038/nsmb.2501.

Berti, M., Cortez, D., and Lopes, M. (2020). The plasticity of DNA replication forks in response to clinically relevant genotoxic stress. Nat. Rev. Mol. Cell Biol. *21*, 633–651. https://doi.org/10.1038/s41580-020-0257-5.

Betous, R., Couch, F., Mason, A., Eichman, B., Manosas, M., and Cortez, D. (2013). Substrate-selective repair and restart of replication forks by DNA translocases. Cell Rep. *3*, 1958. https://doi.org/10.1016/j.celrep.2013.05.002.

Boyer, S.W., Rajendiran, S., Beaudin, A.E., Smith-Berdan, S., Muthuswamy, P.K., Perez-Cunningham, J., Martin, E.W., Cheung, C., Tsang, H., Landon, M., and Forsberg, E.C. (2019). Clonal and Quantitative In Vivo Assessment of Hematopoietic Stem Cell Differentiation Reveals Strong Erythroid Potential of Multipotent Cells. Stem Cell Rep. *12*, 801–815. https://doi.org/10.1016/j.stemcr.2019.02.007.

Busch, K., Klapproth, K., Barile, M., Flossdorf, M., Holland-Letz, T., Schlenner, S.M., Reth, M., Höfer, T., and Rodewald, H.-R. (2015). Fundamental properties of unperturbed haematopoiesis from stem cells in vivo. Nature *518*, 542–546. https://doi.org/10.1038/nature14242.

Ray Chaudhuri, A., Hashimoto, Y., Herrador, R., Neelsen, K.J., Fachinetti, D., Bermejo, R., Cocito, A., Costanzo, V., and Lopes, M. (2012). Topoisomerase I poisoning results in PARP-mediated replication fork reversal. Nat. Struct. Mol. Biol. *19*, 417–423. https://doi.org/10.1038/nsmb.2258.

Cheshier, S.H., Prohaska, S.S., and Weissman, I.L. (2007). The Effect of Bleeding on Hematopoietic Stem Cell Cycling and Self-Renewal. Stem Cells Dev *16*, 707–718. https://doi.org/10.1089/scd.2007.0017.

Christodoulou, C., Spencer, J.A., Yeh, S.-C.A., Turcotte, R., Kokkaliaris, K.D., Panero, R., Ramos, A., Guo, G., Seyedhassantehrani, N., Esipova, T.V., et al. (2020). Live-animal imaging of native hematopoietic stem and progenitor cells. Nature *578*, 278–283. https://doi.org/10.1038/s41586-020-1971-z.

Cortez, D. (2019). Replication-Coupled DNA Repair. Mol Cell *74*, 866–876. https://doi.org/10.1016/j.molcel.2019.04.027.

Essers, M.A.G., Offner, S., Blanco-Bose, W.E., Waibler, Z., Kalinke, U., Duchosal, M.A., and Trumpp, A. (2009). IFNα activates dormant hematopoietic stem cells in vivo. Nature *458*, 904–908. https://doi.org/10.1038/nature07815.

Flach, J., Bakker, S.T., Mohrin, M., Conroy, P.C., Pietras, E.M., Reynaud, D., Alvarez, S., Diolaiti, M.E., Ugarte, F., Forsberg, E.C., et al. (2014). Replication stress is a potent driver of functional decline in ageing hematopoietic stem cells. Nature *512*, 198–202. https://doi.org/10.1038/nature13619.

Follonier, C., Oehler, J., Herrador, R., and Lopes, M. (2013). Friedreich's ataxia–associated GAA repeats induce replication-fork reversal and unusual molecular junctions. Nat. Struct. Mol. Biol. *20*, 486–494. https://doi.org/10.1038/nsmb.2520.

Foudi, A., Hochedlinger, K., Van Buren, D., Schindler, J.W., Jaenisch, R., Carey, V., and Hock, H. (2009). Analysis of histone 2B-GFP retention reveals slowly cycling hematopoietic stem cells. Nat. Biotechnol. *27*, 84–90. https://doi.org/10.1038/nbt.1517.

Garaycoechea, J.I., Crossan, G.P., Langevin, F., Daly, M., Arends, M.J., and Patel, K.J. (2012). Genotoxic consequences of endogenous aldehydes on mouse hematopoietic stem cell function. Nature *489*, 571–575. https://doi.org/10.1038/nature11368.

Garaycoechea, J.I., Crossan, G.P., Langevin, F., Mulderrig, L., Louzada, S., Yang, F., Guilbaud, G., Park, N., Roerink, S., Nik-Zainal, S., et al. (2018). Alcohol and endogenous aldehydes damage chromosomes and mutate stem cells. Nature *553*, 171–177. https://doi.org/10.1038/nature25154.

García-Gómez, S., Reyes, A., Martínez-Jiménez, M., Chocrón, E., Mourón, S., Terrados, G., Powell, C., Salido, E., Mendez, J., Holt, I., and Blanco, L. (2013). PrimPol, an archaic primase/polymerase operating in human cells. Mol Cell *52*, 541–553. https://doi.org/10.1016/j.molcel.2013.09.025.

González-Acosta, D., Blanco-Romero, E., Ubieto-Capella, P., Mutreja, K., Míguez, S., Llanos, S., García, F., Muñoz, J., Blanco, L., Lopes, M., and Mendez, J. (2021). PrimPol-mediated repriming facilitates replication traverse of DNA interstrand crosslinks. Embo J *40*, e106355. https://doi.org/10.15252/embj.2020106355.

Guilliam, T., and Doherty, A. (2017). PrimPol-Prime Time to Reprime. Genes *8*, 20. https://doi.org/10.3390/genes8010020.

Hampp, S., Kiessling, T., Buechle, K., Mansilla, S.F., Thomale, J., Rall, M., Ahn, J., Pospiech, H., Gottifredi, V., and Wiesmüller, L. (2016). DNA damage tolerance pathway involving DNA polymerase ι and the tumor suppressor p53 regulates DNA replication fork progression. P Natl Acad Sci Usa *113*, E4311–E4319. https://doi.org/10.1073/pnas.1605828113.

Hatakeyama, M., Opitz, L., Russo, G., Qi, W., Schlapbach, R., and Rehrauer, H. (2016). SUSHI: an exquisite recipe for fully documented, reproducible and reusable NGS data analysis. BMC Bioinf. *17*, 228. https://doi.org/10.1186/s12859-016-1104-8.

Huntly, B.J., Shigematsu, H., Deguchi, K., Lee, B.H., Mizuno, S., Duclos, N., Rowan, R., Amaral, S., Curley, D., Williams, I.R., et al. (2004). MOZ-TIF2, but not BCR-ABL, confers properties of leukemic stem cells to committed murine hematopoietic progenitors. Cancer Cell *6*, 587–596. https://doi.org/10.1016/j.ccr.2004.10.015.

Jacobs, K., Van de Velde, H., De Paepe, C., Sermon, K., and Spits, C. (2017). Mitotic spindle disruption in human preimplantation embryos activates the spindle assembly checkpoint but not apoptosis until Day 5 of development. Mol. Hum. Reprod. *23*, 321–329. https://doi.org/10.1093/molehr/gax007.

Kiel, M.J., Yilmaz, Ö.H., Iwashita, T., Yilmaz, O.H., Terhorst, C., and Morrison, S.J. (2005). SLAM Family Receptors Distinguish Hematopoietic Stem and Progenitor Cells and Reveal Endothelial Niches for Stem Cells. Cell *121*, 1109–1121. https://doi.org/10.1016/j.cell.2005.05.026.

Kiessling, A.A. (2010). Timing is everything in the human embryo. Nat. Biotechnol. *28*, 1025–1026. https://doi.org/10.1038/nbt1010-1025.

Kobayashi, K., Guilliam, T.A., Tsuda, M., Yamamoto, J., Bailey, L.J., Iwai, S., Takeda, S., Doherty, A.J., and Hirota, K. (2016). Repriming by PrimPol is critical for DNA replication restart downstream of lesions and chain-terminating nucleosides. Cell Cycle *15*, 1997–2008. https://doi.org/10.1080/15384101.2016.1191711.

Kolinjivadi, A.M., Sannino, V., De Antoni, A., Zadorozhny, K., Kilkenny, M., Técher, H., Baldi, G., Shen, R., Ciccia, A., Pellegrini, L., et al. (2017). Smarcal1-Mediated Fork Reversal Triggers Mre11-Dependent Degradation of Nascent DNA in the Absence of Brca2 and Stable Rad51 Nucleofilaments. Mol Cell *67*, 867–881.e7. https://doi.org/10.1016/j.molcel.2017.07.001.

Langevin, F., Crossan, G.P., Rosado, I.V., Arends, M.J., and Patel, K.J. (2011). Fancd2 counteracts the toxic effects of naturally produced aldehydes in mice. Nature *475*, 53–58. https://doi.org/10.1038/nature10192.

Laurenti, E., and Göttgens, B. (2018). From hematopoietic stem cells to complex differentiation landscapes. Nature *553*, 418–426. https://doi.org/10.1038/nature25022.

Lawrence, M., Huber, W., Pagès, H., Aboyoun, P., Carlson, M., Gentleman, R., Morgan, M.T., and Carey, V.J. (2013). Software for Computing and Annotating Genomic Ranges. PLoS Comput. Biol. *9*, e1003118. https://doi.org/10.1371/journal.pcbi.1003118.

Macheret, M., and Halazonetis, T.D. (2015). DNA replication stress as a hallmark of cancer. Annu. Rev. Pathol. *10*, 425–448. https://doi.org/10.1146/annurev-pathol-012414-040424.

Matatall, K.A., Jeong, M., Chen, S., Sun, D., Chen, F., Mo, Q., Kimmel, M., and King, K.Y. (2016). Chronic Infection Depletes Hematopoietic Stem Cells through Stress-Induced Terminal Differentiation. Cell Rep. *17*, 2584–2595. https://doi.org/10.1016/j.celrep.2016.11.031.

Maya-Mendoza, A., Moudry, P., Merchut-Maya, J.M., Lee, M., Strauss, R., and Bartek, J. (2018). High speed of fork progression induces DNA replication stress and genomic instability. Nature *559*, 279–284. https://doi.org/10.1038/s41586-018-0261-5.

Mayle, A., Luo, M., Jeong, M., and Goodell, M.A. (2013). Flow cytometry analysis of murine hematopoietic stem cells. Cytom Part A *83A*, 27–37. https://doi.org/10.1002/cyto.a.22093.

McCormack, M.P., Young, L.F., Vasudevan, S., de Graaf, C.A., Codrington, R., Rabbitts, T.H., Jane, S.M., and Curtis, D.J. (2010). The Lmo2 Oncogene Initiates Leukemia in Mice by Inducing Thymocyte Self-Renewal. Science *327*, 879–883. https://doi.org/10.1126/science.1182378.

Mohrin, M., Bourke, E., Alexander, D., Warr, M.R., Barry-Holson, K., Le Beau, M.M., Morrison, C.G., and Passegue, E. (2010). Hematopoietic stem cell quiescence promotes error-prone DNA repair and mutagenesis. Cell Stem Cell *7*, 174–185. https://doi.org/10.1016/j.stem.2010.06.014.

Morrison, S.J., Wright, D.E., and Weissman, I.L. (1997). Cyclophosphamide/granulocyte colony-stimulating factor induces hematopoietic stem cells to proliferate prior to mobilization. Proc National Acad Sci *94*, 1908–1913. https://doi.org/10.1073/pnas.94.5.1908.

Mourón, S., Rodriguez-Acebes, S., Martínez-Jiménez, M.I., García-Gómez, S., Chocrón, S., Blanco, L., and Mendez, J. (2013). Repriming of DNA synthesis at stalled replication forks by human PrimPol. Nat. Struct. Mol. Biol. *20*, 1383–1389. https://doi.org/10.1038/nsmb.2719.

Mun, Y., and Nombela-Arrieta, C. (2021). 3D Microscopy of Murine Bone Marrow Hematopoietic Tissues. Methods Mol Biology Clifton N J *2308*, 127–138. https://doi.org/10.1007/978-1-0716-1425-9_11.

Nakatani, T., Lin, J., Ji, F., Ettinger, A., Pontabry, J., Tokoro, M., Altamirano-Pacheco, L., Fiorentino, J., Mahammadov, E., Hatano, Y., et al. (2022). DNA replication fork speed underlies cell fate changes and promotes reprogramming. Nat. Genet. *54*, 318–327. https://doi.org/10.1038/s41588-022-01023-0.

Neelsen, K.J., Zanini, I.M., Herrador, R., and Lopes, M. (2013). Oncogenes induce genotoxic stress by mitotic processing of unusual replication intermediates. J. Cell Biol. *200*, 699–708. https://doi.org/10.1128/mcb.24.16.7140-7150.2004.

Orford, K.W., and Scadden, D.T. (2008). Deconstructing stem cell self-renewal: genetic insights into cell-cycle regulation. Nat. Rev. Genet. *9*, 115–128. https://doi.org/10.1038/nrg2269.

Piberger, A.L., Bowry, A., Kelly, R.D.W., Walker, A.K., González-Acosta, D., Bailey, L.J., Doherty, A.J., Méndez, J., Morris, J.R., Bryant, H.E., and Petermann, E. (2020). PrimPol-dependent single-stranded gap formation

mediates homologous recombination at bulky DNA adducts. Nat. Commun. *11*, 5863. https://doi.org/10.1038/s41467-020-19570-7.

Puccetti, M.V., Fischer, M.A., Arrate, M.P., Boyd, K.L., Duszynski, R.J., Betous, R., Cortez, D., and Eischen, C.M. (2017). Defective replication stress response inhibits lymphomagenesis and impairs lymphocyte reconstitution. Oncogene *36*, 2553–2564. https://doi.org/10.1038/onc.2016.408.

Puccetti, M.V., Adams, C.M., Kushinsky, S., and Eischen, C.M. (2019). Smarcal1 and Zranb3 Protect Replication Forks from Myc-Induced DNA Replication Stress. Cancer Res. *79*, 1612–1623. https://doi.org/10.1158/0008-5472.can-18-2705.

Quinet, A., Carvajal-Maldonado, D., Lemacon, D., and Vindigni, A. (2017). DNA Fiber Analysis: Mind the Gap. Meth. Enzymol. *591*, 55–82. https://doi.org/10.1016/bs.mie.2017.03.019.

Quinet, A., Tirman, S., Jackson, J., Šviković, S., Lemacon, D., Carvajal-Maldonado, D., González-Acosta, D., Vessoni, A.T., Cybulla, E., Wood, M., et al. (2020). PRIMPOL-Mediated Adaptive Response Suppresses Replication Fork Reversal in BRCA-Deficient Cells. Mol Cell *77*, 461–474.e9. https://doi.org/10.1016/j.molcel.2019.10.008.

Rieger, M.A., and Schroeder, T. (2012). Hematopoiesis. Csh Perspect Biol *4*, a008250. https://doi.org/10.1101/cshperspect.a008250.

Robinson, M.D., McCarthy, D.J., and Smyth, G.K. (2010). edgeR: a Bioconductor package for differential expression analysis of digital gene expression data. Bioinformatics *26*, 139–140. https://doi.org/10.1093/bioinformatics/btp616.

Rossi, D.J., Bryder, D., Seita, J., Nussenzweig, A., Hoeijmakers, J., and Weissman, I.L. (2007). Deficiencies in DNA damage repair limit the function of hematopoietic stem cells with age. Nature *447*, 725–729. https://doi.org/10.1038/nature05862.

Rossi, D.J., Jamieson, C.H., and Weissman, I.L. (2008). Stems Cells and the Pathways to Aging and Cancer. Cell *132*, 681–696. https://doi.org/10.1016/j.cell.2008.01.036.

Schmid, J.A., Berti, M., Walser, F., Raso, M.C., Schmid, F., Krietsch, J., Stoy, H., Zwicky, K., Ursich, S., Freire, R., et al. (2018). Histone Ubiquitination by the DNA Damage Response Is Required for Efficient DNA Replication in Unperturbed S Phase. Mol Cell *71*, 897–910.e8. https://doi.org/10.1016/j.molcel.2018.07.011.

Smith, C.C., O'Donovan, M.R., and Martin, E.A. (2006). hOGG1 recognizes oxidative damage using the comet assay with greater specificity than FPG or ENDOIII. Mutagenesis *21*, 185–190. https://doi.org/10.1093/mutage/gel019.

Stambrook, P.J., and Tichy, E.D. (2010). Preservation of genomic integrity in mouse embryonic stem cells. Adv. Exp. Med. Biol. *695*, 59–75. https://doi.org/10.1007/978-1-4419-7037-4_5.

Sun, J., Ramos, A., Chapman, B., Johnnidis, J.B., Le, L., Ho, Y.-J., Klein, A., Hofmann, O., and Camargo, F.D. (2014). Clonal dynamics of native haematopoiesis. Nature *514*, 322–327. https://doi.org/10.1038/nature13824.

Taniguchi, T., and D'Andrea, A.D. (2006). Molecular pathogenesis of Fanconi anemia: recent progress. Blood *107*, 4223–4233. https://doi.org/10.1182/blood-2005-10-4240.

Thangavel, S., Berti, M., Levikova, M., Pinto, C., Gomathinayagam, S., Vujanovic, M., Zellweger, R., Moore, H., Lee, E.H., Hendrickson, E.A., et al. (2015). DNA2 drives processing and restart of reversed replication forks in human cells. J. Cell Biol. *208*, 545–562. https://doi.org/10.1083/jcb.201406100.

Tomasetti, C., Durrett, R., Kimmel, M., Lambert, A., Parmigiani, G., Zauber, A., and Vogelstein, B. (2017). Role of stem-cell divisions in cancer risk. Nature *548*, E13–E14. https://doi.org/10.1038/nature23302.

Tothova, Z., Kollipara, R., Huntly, B.J., Lee, B.H., Castrillon, D.H., Cullen, D.E., McDowell, E.P., Lazo-Kallanian, S., Williams, I.R., Sears, C., et al. (2007). FoxOs Are Critical Mediators of Hematopoietic Stem Cell Resistance to Physiologic Oxidative Stress. Cell *128*, 325–339. https://doi.org/10.1016/j.cell.2007.01.003.

Vetrie, D., Helgason, G.V., and Copland, M. (2020). The leukaemia stem cell: similarities, differences and clinical prospects in CML and AML. Nat. Rev. Cancer *20*, 158–173. https://doi.org/10.1038/s41568-019-0230-9.

Visvader, J.E. (2011). Cells of origin in cancer. Nature *469*, 314–322. https://doi.org/10.1038/nature09781.

Vujanovic, M., Krietsch, J., Raso, M.C., Terraneo, N., Zellweger, R., Schmid, J.A., Taglialatela, A., Huang, J.-W., Holland, C.L., Zwicky, K., et al. (2017). Replication Fork Slowing and Reversal upon DNA Damage Require PCNA Polyubiquitination and ZRANB3 DNA Translocase Activity. Mol Cell *67*, 882–890.e5. https://doi.org/10.1016/j.molcel.2017.08.010.

Walter, D., Lier, A., Geiselhart, A., Thalheimer, F.B., Huntscha, S., Sobotta, M.C., Moehrle, B., Brocks, D., Bayindir, I., Kaschutnig, P., et al. (2015). Exit from dormancy provokes DNA-damage-induced attrition in hematopoietic stem cells. Nature *520*, 549–552. https://doi.org/10.1038/nature14131.

Wilson, A., Laurenti, E., Oser, G., van der Wath, R.C., Blanco-Bose, W., Jaworski, M., Offner, S., Dunant, C.F., Eshkind, L., Bockamp, E., et al. (2008). Hematopoietic stem cells reversibly switch from dormancy to self-renewal during homeostasis and repair. Cell *135*, 1118–1129. https://doi.org/10.1016/j.cell.2008.10.048.

Wong, C.C., Loewke, K.E., Bossert, N.L., Behr, B., De Jonge, C.J., Baer, T.M., and Pera, R.A.R. (2010). Non-invasive imaging of human embryos before embryonic genome activation predicts development to the blastocyst stage. Nat. Biotechnol. *28*, 1115–1121. https://doi.org/10.1038/nbt.1686.

Wu, S., Powers, S., Zhu, W., and Hannun, Y.A. (2016). Substantial contribution of extrinsic risk factors to cancer development. Nature *529*, 43–47. https://doi.org/10.1038/nature16166.

Yang, L., Bryder, D., Adolfsson, J., Nygren, J., Månsson, R., Sigvardsson, M., and Jacobsen, S.E.W. (2005). Identification of Lin–Sca1+kit+CD34+Flt3– short-term hematopoietic stem cells capable of rapidly reconstituting and rescuing myeloablated transplant recipients. Blood *105*, 2717–2723. https://doi.org/10.1182/blood-2004-06-2159.

Zellweger, R., and Lopes, M. (2017). Genome Instability (New York: Springer).

Zellweger, R., Dalcher, D., Mutreja, K., Berti, M., Schmid, J.A., Herrador, R., Vindigni, A., and Lopes, M. (2015). Rad51-mediated replication fork reversal is a global response to genotoxic treatments in human cells. J. Cell Biol. *208*, 563–579. https://doi.org/10.1083/jcb.201406099.

Zeman, M.K., and Cimprich, K.A. (2014). Causes and consequences of replication stress. Nat. Cell Biol. *16*, 2–9. https://doi.org/10.1038/ncb2897.

STAR★METHODS

KEY RESOURCES TABLE

REAGENT or RESOURCE	SOURCE	IDENTIFIER
Antibodies		
Purified anti-mouse CD3	Biolegend	Cat#: 100,202; RRID: AB_312659
Purified anti-mouse CD4	Biolegend	Cat#: 100,402; RRID:AB_312687
Purified anti-mouse CD5	Biolegend	Cat#: 100,602; RRID:AB_312731
Purified anti-mouse CD8a	Biolegend	Cat#: 100,702; RRID:AB_312741
Purified anti-mouse Ly-6G/Ly-6C (Gr-1)	Biolegend	Cat#: 108,402; RRID:AB_313367
Purified anti-mouse/human CD11b	Biolegend	Cat#: 101,202; RRID:AB_312785
Purified anti-mouse TER-119/Erythroid Cells	Biolegend	Cat#: 116,202; RRID:AB_313703
Purified anti-mouse/human CD45R/B220	Biolegend	Cat#: 103,202; RRID:AB_312987
F(ab')2-Goat anti-Rat IgG (H L) Secondary Antibody Cy5	Invitrogen	Cat#: A10691; RRID:AB_2534067
APC/Cyanine7 anti-mouse CD117 (c-kit)	Biolegend	Cat#: 105,826; RRID:AB_1626278
Pacific Blue™ anti-mouse Ly-6A/E (Sca-1)	Biolegend	Cat#: 108,120; RRID:AB_493273
PE/Cyanine7 anti-mouse CD150 (SLAM) Antibody	Biolegend	Cat#: 115,914; RRID:AB_439797
CD135 (Flt3) Monoclonal Antibody (A2F10), Biotin	Biolegend	Cat#: 13-1351-85; RRID:AB_466600
CD34 FITC	Invitrogen	Cat#: 11-0341-82; RRID:AB_465021
Qdot 605 Streptavidin Conjugate-200 μL	Invitrogen	Cat#: Q10101MP
FC block (CD16/CD32)	BD PharmingenTM	RRID: AB_394656
Ly6G/Ly6C (Gr1)-Biotin	BD Biosciences	Cat#: RB6-8C5
CD45.2-PERCP-CY5.5 (104)	BD PharmingenTM	RRID: AB_953590
CD45.1-APC	BD PharmingenTM	RRID: Ab_1645214
CD3e-BV711	BD Biosciences	RRID: AB_2687954
B220-FITC (RA3-6B2)	BD Biosciences	RRID: AB_394618
CD11b-V450 (M1/70)	Tonbo	Cat#: 75-0112
BUV661 Mouse Anti-Mouse CD45.1 (A20) (RUO)	BD Bioscience	Cat#: 741,517; RRID: AB_2870966
Rat anti-mouse Lineage cocktail BV421 clone 17.A2	BioLegend	Cat#: 133,311
Brilliant Violet 785™ anti-mouse CD150 (SLAM)	BioLegend	Cat#: 115,937
Ly-6A/E (Sca-1) Monoclonal Antibody (D7), FITC, eBioscience™	Invitrogen	Cat#: 11-5981-82; RRID: AB_465333
PerCP-Cy™5.5 Mouse Anti-Mouse CD45.2	BD Pharmigen	Cat#: 552,950; RRID: AB_394528
Rat anti-mouse CD34 PE clone RAM34	BD Pharmingen	Cat#: 551,387; RRID: AB_394176

(*Continued on next page*)

Continued

REAGENT or RESOURCE	SOURCE	IDENTIFIER
APC anti-mouse CD135	BioLegend	Cat#: 135,309
Rat anti-mouse cKit (CD117) APC-H7 clone 2B8	BD Pharmingen	Cat#: 560,185; RRID: AB_1645231
DAPI	ThermoFisher	Cat#: 62,248
SA-PECY7	BD Pharmingen	RRID: AB_10049577
CD117 Micro-Beads	Miltenyi Biotec	Cat#: 130-091-224; RRID:AB_2753213
Mouse anti-γH2AX	Milipore	Cat#: 05-636-I; RRID:AB_2755003
Rabbit anti-53BP1	Novusbio	Cat#: NB100-305SS; RRID:AB_920464
Anti-rabbit Alexa Fluor 546	ThermoFisher Scientific	Cat#: A11035; RRID:AB_2534093
Alexa Fluor 488 Goat anti-Mouse IgG (H + L) Cross-Adsorbed Secondary Antibody	ThermoFisher Scientific	Cat#: A11001; RRID:AB_2534069
Cy™3 AffiniPure F(ab')₂ Fragment Donkey Anti-Rat IgG (H + L)	Jackson ImmunoResearch Laboratories, Inc.	Cat#: 712-166-153; RRID:AB_2340669
Rabbit anti-PrimPol	This paper; R. Freire lab Instituto de Tecnologías Biomédicas, Tenerife, Spain	N/A
Mouse anti-SMARCAL1	Santa Cruz	Cat#: sc-376377; RRID:AB_10987841
Mouse anti-biotin	Jackson ImmunoResearch Laboratories, Inc.	Cat#: 200-002-211; RRID:AB_2339006
Rabbit anti-biotin	Abcam	Cat#: ab53494; RRID:AB_867860
Rat anti-BrdU/CldURat monoclonal [BU1/75 (ICR1)] to BrdU	Abcam	Cat#: ab6326-100UG; RRID:AB_305426
Chemicals, peptides, and recombinant proteins		
5-Chloro-2′-deoxyuridine	Sigma-Aldrich	Cat #: C6891-100MG
5-Iodo-2′-deoxyuridine	Sigma-Aldrich	Cat #: I7125
Poly(I:C) (HMW), 50mg	InvivoGen	Cat #: tlrl-pic-5
Murine IFNα	Miltenyi Biotec	Cat#:130-093-131
StemSpan™ SFEM (100mL)	STEMCELL Technologies	Cat#: 9600
Penicillin-Streptomycin sterile filtered 100mL	Sigma	Cat#: 7,002,243
Recombinant Murine TPO, 10ug	Bioconcept	Cat#: 315-14
Stem Cell Factor (SCF)	Bioconcept	Cat#: CLY200-09-500UG
Palbociclib (PD-0332991) HCl	Lubioscience	Cat#: S1116-50MG
5-ethynyl-2′-deoxyuridine (EdU)	ThermoFisher Scientific	Cat#: A10044
N-acetyl-L-cysteine	Sigma	Cat#: A7250-5G
Neocarzinostatin (NCS)	Sigma	Cat#: N9162-100UG
Poly-L-lysine	Sigma	Cat#: P4832-50mL
Alexa Fluor™ 647 Azide	ThermoFisher Scientific	Cat#: A10277
Biotin azide	Vanderbilt University	Cat#: 1,284,538
SeaPlaque low-melting point agarose	Lonza	Cat#: 50,111
SYBR™ Gold Nucleic Acid Gel Stain (100,00X Concentrate in DMSO)	ThermoFisher Scientific	Cat#: S11494
S1 Nuclease (100 U/μL)	ThermoFisher Scientific	Cat#: 18,001,016
DNAse I	NEB	Cat#: M0303S

(*Continued on next page*)

Continued

REAGENT or RESOURCE	SOURCE	IDENTIFIER
Camptothecin	Sigma Aldrich	Cat#: C9911-100mg
Proteinase K	Sigma	Cat#: 3,115,852,001
4 5 8 Trimethylpsoralen, 1 gramm	Sigma	Cat#: T6137-1G
PvuII-HF, 25′000units	New England Biolabs	Cat#: R3151L
Neomycin	Sigma	Cat#: N1142
Critical commercial assays		
hOGG1 FLARE™ Assay Kit	Trevigen	Cat#: 4130-100-FK
Click-iT EdU Alexa Fluor 647 Imaging Kit (Immunofluorescence)	Thermo Fisher Scientific	Cat#: C10640
RNeasy Micro Kit	Qiagen	Cat#: 74,004
Duolink® *In Situ* PLA® reagents far-red	Sigma	Cat#: DUO92013-100RXN
Duolink® *In Situ* PLA® Probe Anti-Rabbit MINUS	Sigma	Cat#: DUO92005-100RXN
Duolink® *In Situ* PLA® Probe Anti-Mouse PLUS	Sigma	Cat#: DUO92001-100RXN
LIVE/DEAD Yellow fixable	ThermoFisher	Cat#:L34959
Deposited data		
Raw data and analyzed data	this paper	https://doi.org/10.17632/xx6f9629hf.1
RNAseq data:	this paper	GEO: GSE212580
Experimental models: Cell lines		
53BP1 KO MEFs	Ross Chapman lab, University of Oxford and Andre Nussenzweig lab, NIH National Cancer institute	N/A
Primary SMARCAL1 KO MEFs	Christine Eischen lab, Thomas Jefferson University	N/A
Experimental models: Organisms/strains		
Mouse C57Bl/6JRj	Janvier	N/A
Mouse C57Bl/6 Smarcal$^{+/\Delta}$	Dr. Cornelius Boerkel (University of British Columbia, USA)	N/A
Mouse C57Bl/6 Zranb3$^{+/-}$	Texas Institute of Genomic Medicine (TIGM, Fort Worth, TX, USA)	N/A
Mouse C57Bl/6 Primpol$^{+/-}$	Dr. Juan Mendez, Spanish National Cancer Research Center (CNIO)	N/A
Mouse C57BL/6N Fanca$^{+/-}$	Dr. KJ Patel (MRC Laboratory of Molecular Biology, Cambridge University)	N/A
Mouse C57Bl/6 wt (host for BMT experiments)	Dr. Juan Mendez, Spanish National Cancer Research Center (CNIO)	N/A
Software and algorithms		
GraphPad Prism 8 for MAC OS X	GraphPad Software	https://www.graphpad.com/scientific-software/prism/
ImageJ Version 2.0.0-rc-69/1.52p (DNA fiber length analysis and comet assay scoring)	ImageJ Software	https://ImageJ.nih.gov/ij/download.html
OpenComet plugin Version 1.3.1	OpenComet Software	https://cometbio.org/
FlowJo (Facs data analysis)	FlowJo Software	https://www.flowjo.com/solutions/flowjo
CellProfiler-3.1.8 (IF and PLA data analysis)	CellProfiler Software	https://cellprofiler.org/
Olympus ScanR Image Analysis Software Version 2.5.1 (QIBC data analysis)	Olympus Corporation	https://www.olympus-ims.com/en/microscope/software/
Spotfire data visualization software version 5.0.0 (QIBC data analysis)	TIBCO Software Inc.	https://www.tibco.com/

(*Continued on next page*)

Continued

REAGENT or RESOURCE	SOURCE	IDENTIFIER
FusionCapt Advance Solo 7 17.02 control and analysis software for chemiluminescence detection (used for western blot)	Vilber Lourmat	https://www.vilber.com/
R and SUSHI	RNAseq data analysis	https://bmcbioinformatics.biomedcentral.com/articles/10.1186/s12859-016-1104-8
DigitalMicrograph version 1.83.842	Gatan, Inc.	https://www.gatan.com/products/tem-analysis/gatan-microscopy-suite-software
Biorender	Graphical abstract	https://app.biorender.com/
BD FACS DIVA Software (FACS data acquisition)	DIVA Software	https://www.bdbiosciences.com/en-eu/products/software/instrument-software/bd-facsdiva-software

RESOURCE AVAILABILITY

Lead contact

Further information and requests for resources and reagents should be directed to and will be fulfilled by the lead contact, Massimo Lopes (lopes@imcr.uzh.ch).

Materials availability

The antibody directed against Primpol generated for this study will be made available upon request by Massimo Lopes (lopes@imcr.uzh.ch).

Data and code availability

- All original, uncropped images and other raw data used to build main and supplemental figures have been deposited in Mendeley: https://doi.org/10.17632/xx6f9629hf.1.
- RNA-seq raw data have been deposited in GEO: GSE212580.
- This paper does not report original code.
- Any additional information required to reanalyze the data reported in this paper is available from the lead contact upon request.

EXPERIMENTAL MODEL AND SUBJECT DETAILS

Mouse models

C57Bl/6JRj WT mice were obtained from Janvier Labs and maintained in individually ventilated cages in accredited animal facilities at the University of Zürich, Switzerland. C57Bl/6 *Primpol*$^{+/-}$ mice were derived, bred at the Spanish National Cancer Research Center (CNIO), Madrid, Spain and imported via embryo transfer and bred in accredited animal facilities at the University of Zürich. C57BL/6N Fanca$^{+/-}$ were kindly provided by Dr. KJ Patel (MRC Laboratory of Molecular Biology, Cambridge University) and bred in accredited animal facilities at the University of Zürich.

Experiments with C57Bl/6JRj WT, C57Bl/6 Primpol$^{+/-}$, Fanca$^{+/-}$ mice were conducted in accredited animal facilities at the University of Zürich, Switzerland at University Zürich and were priorly approved by the appropriate ethical committees (licenses number 28366 and 31,551). Male and female mice at 8–12 weeks of age for wt-only studies, and 8-18 weeks for the age-matched controlled knockout mice studies were used.

Smarcal$^{+/\Delta}$ mice were previously provided by Dr. Cornelius Boerkel (University of British Columbia). *Zranb3*$^{+/-}$ founder mice were purchased from the Texas Institute of Genomic Medicine (TIGM, Fort Worth, TX). *Smarcal1*$^{+/\Delta}$ and *Zranb3*$^{+/-}$ mice were backcrossed 12 generations onto a C57Bl/6 background and were further bred and maintained at Thomas Jefferson University, Philadelphia, USA.

Experiments with C57Bl/6 Smarcal1$^{\Delta/\Delta}$, C57Bl/6 *Zranb3*$^{-/-}$ and C57Bl/6 wild-type mice were approved by the Animal Care and Use Committee at Thomas Jefferson University (#01770). Both males and females (9-15 weeks old) were used for Smarcal1 knockout and Zranb3 knockout mice and their WT age-matched controls.

Experiments with C57Bl/6 Primpol$^{+/-}$ mice at the Spanish National Cancer Research Center (CNIO), Madrid, Spain were approved by the CNIO and CNIC Ethics Committees and the Madrid regional authorities (PROEX 015/16 and PROEX 327.6/21) and conformed to European Union (EU) Directive 2010/63/EU and Recommendation 2007/526/EC regarding the protection of animals used for experimental and other scientific purposes, enforced in Spanish law under Real Decreto 120½005. Male and female mice at

8-18 weeks for the age-matched controlled knockout mice studies were used. Male and female host mice for the BMT experiment were 6-8 weeks.

METHOD DETAILS

Mouse manipulations and group sizes

Mice were included in experiments at 8–12 weeks of age for wt-only studies, and 8-18 weeks for the age-matched controlled knockout mice studies. Animals were injected with 5 mg/kg pI:pC (InvivoGen) intraperitoneally (i.p.) or 2×10^5 units recombinant murine IFNα (Miltenyi) subcutaneously (s.c.), 48 h before bone marrow isolation, or with 100μL PBS as negative control. For *in vitro* stimulation, cells were cultured 48 h in StemSpan SFEM medium (STEMCELL Technologies), supplemented with 1% penicillin/streptomycin, 2% L-glutamine 100 ng/mL, Thrombopoietin (Bioconcept) and 100 ng/mL Stem Cell Factor (Bioconcept). The complemented medium was exchanged once after 24 h in culture.

Palbociclib (20 mg/kg, PD0332991 HCl) (Lubioscience) was injected intravenously (i.v.) at the indicated timepoints. 5-ethynyl-2′-deoxyuridine (EdU) (25 mg/kg, ThermoFisher Scientific) was injected i.v. 45 min before sacrifice in the relevant experiments. Where stated, drinking water was supplemented with 1 g/L N-acetyl-L-cysteine (Sigma) for 14 days prior to bone marrow isolation, during which water intake and mouse weight was controlled. Animals were sacrificed using CO_2.

Animal group sizes per experimental condition were as follows:

Cell cycle experiments, comet and fiber assays: untreated/PBS n = 3, pI:pC n = 2, INFα n = 2. Combined IF and comet experiments: untreated/PBS n = 8, pI:pC = 6. PLA experiments: untreated/PBS n = 6, pI:pC = 4. Cell counting experiments: each for wt and PrimPol$^{-/-}$ untreated/PBS n = 7 and pI:pC n = 7. Competitive transplantation experiments: donor mice n = 6 and recipient mice n = 24.

Isolation of hematopoietic cell subsets

Femora, tibiae and ilia were isolated and gently crushed in staining medium (PBS + 5mM EDTA +2% fetal bovine serum). Unless stated otherwise, for each untreated (−) sample, the bone marrow of 3 mice were pooled, and for each pI:pC sample the bone marrow of 2 mice were pooled, to increase sample size and to decrease artifacts based on mouse-to-mouse variability. Red blood cells (RBCs) were lysed using Ammonium-Chloride-Potassium (ACK) lysing buffer for 1min on ice. CD117 (c-KIT) positive cells were enriched using CD117 Micro-Beads (Miltenyi Biotec) and subsequently immunostained using the antibodies listed here below. Propidium Iodide (ThermoFisher Scientific) was used for negative selection of dead cells. All sorting experiments were performed using BD FACSAria II or III flow cytometer (BD Biosciences), using the gating strategy illustrated in Figure S1A. Antibodies used for FACS sorting of hematopoietic bone marrow cells: CD3 (Biolegend), CD4 (Biolegend), CD5 (Biolegend), CD8 (Biolegend), Gr1 (Biolegend), CD11b (Biolegend), Ter119 (Biolegend, B220 (Biolegend), anti-rat PeCy5 (Invitrogen), c-kit APC-Cy7 (Biolegend), Sca1 Pacific Blue (Biolegend), SLAM PeCy7 (Biolegend), Flk2 Biotin (Biolegend), CD34 FITC (Invitrogen), Streptavidine QDot 605 (Invitrogen).

Immunostaining

After isolation, for DNA fiber assay, Immunofluorescence stainings and PLA, cells were left to recover for 30 min in StemSpan SFEM medium (STEMCELL Technologies) and subsequently incubated in 25μM 5-ethynyl-2′-deoxyuridine (EdU, ThermoFisher Scientific) where indicated. Cells were optionally treated with 5 μg/ml NCS (Sigma) for 1h. Cells were subsequently sedimented on poly-L-lysine (Sigma) pre-coated 8-well μ-slides (Ibidi). Cells were pre-fixated in 0.1% formaldehyde (Sigma), pre-extracted using CSK-buffer (10mM 4-(2-hydroxyethyl)-1-piperazineethanesulfonic acid (HEPES) pH = 7.4, 0.1M NaCl, 0.3M sucrose, 3mM $MgCl_2$) for 5 min, fixed for 15 min with 4% formaldehyde (Sigma) and optionally for PrimPol and SMARCAL antibody stainings post-fixated using methanol for 20 min at −20°C. Cells were subsequently blocked using blocking solution (5% BSA +10% fetal bovine serum [FBS]) for 1h and incubated with primary antibodies overnight 4°C for mouse anti-γH2AX (1:800) (Milipore) and rabbit anti-53BP1 (1:500) (Novusbio). After washing with PBS, EdU containing cells were incubated with Click-iT Cell reaction buffer using Alexa Fluor 647 azide. After washing cells are incubated for 1h in blocking solution containing secondary antibodies diluted 1:300: Alexa Fluor 546 anti-Rabbit or Alexa Fluor 488 anti-mouse (ThermoFisher Scientific). After DAPI counterstaining and washing, slides were imaged using a Leica Thunder (64x, oil) and analyzed using CellProfiler. Samples on which only cell-cycle analysis was performed followed the same protocol, except that pre-extraction and antibody incubations were skipped to limit cell-loss.

Antibody validations in MEFs followed the same protocol but cells were seeded on poly-L-lysine coated coverslips.

Quantitative image-based microscopy

Automated multichannel wide-field microscopy for HYPERLINK "https://www.sciencedirect.com/topics/biochemistry-genetics-and-molecular-biology/cytometry" \o "Learn more about QIBC from ScienceDirect's AI-generated Topic Pages" QIBC was performed as described previously (Toledo et al., 2013) on an Olympus ScanR Screening System equipped with wide-field optics, a 20x, 0.75-NA (UPLSAPO 20x), an inverted motorized Olympus IX83 microscope, a motorized stage, IR-laser hardware autofocus, a fast emission filter wheel with single-band emission filters, and a 12-bit digital monochrome Hamamatsu ORCA-FLASH 4.0 V2 sCMOS camera (dynamic range 4,000:1, 2,048 32,948 pixel of size 6.5 3 6.5 mm, 12-bit dynamics). Images were acquired in an automated fashion with the ScanR acquisition software (Olympus 2.6.1). Images were acquired under non-saturating conditions and

identical settings were applied to all samples within one experiment. Images were processed and analyzed with the inbuilt Olympus ScanR Image Analysis Software Version 2.5.1, a dynamic background correction was applied, nuclei segmentation was performed using an integrated intensity-based object detection module using the DAPI signal. Fluorescence intensities were quantified and are depicted as arbitrary units. These values were then exported and analyzed with Spotfire data visualization software (TIBCO, version 5.0.0). To visualize discrete data in scatterplots (e.g., foci numbers), mild jittering (random displacement of data points along the discrete data axes) was applied to demerge overlapping data points.

Proximity ligation assay

Cells were incubated with a 25μM EdU (ThermoFisher Scientific) pulse for 10 min and sedimented on poly-L-lysine (sigma) pre-coated 8-well μ-slides (Ibidi). Cells were pre-fixated in 0.1% formaldehyde (Sigma), pre-extracted using CSK-buffer (10mM HEPES pH = 7.4, 0.1M NaCl, 0.3M sucrose, 3mM $MgCl_2$) for 5 min, fixed for 15 min with 4% formaldehyde (Sigma) and post-fixated using methanol for 20 min at −20°C. After blocking with 5% BSA +10% FBS blocking solution, cells were incubated with Click-iT Cell reaction buffer using azide-Biotin (Vanderbilt University). Afterward, primary antibodies were applied for 1h in blocking solution (see Immunostaining) with either rabbit anti-PrimPol (1:500) – produced in R. Freire's lab immunizing a rabbit with a peptide containing amino acids 1- 240 from murine primpol – or with mouse anti-SMARCAL1 (1:100) (Santa Cruz). Additionally, mouse anti-biotin (1:300)(Jackson ImmunoResearch Laboratories, Inc.) in case of PrimPol SIRF or rabbit anti-biotin (1:2000) (Abcam) in case of SMARCAL1 SIRF were added to the primary antibody solution. Subsequently cells were washed twice for 5 min with buffer A and were then incubated in PLA probe solution for 1h at 37°C, containing 75μL blocking solution, with the addition of each 25μL probe minus and plus for a total of 125μL per well. After washing twice with buffer A, cells were incubated in 121.875μL ligation buffer with the addition of 3.125μL ligation enzyme for a total of 125μL per well, for 30 min at 37°C. After two buffer A washes, cells incubated in amplification solution for 100 min at 37°C. The amplification solution consists of 121.875μL amplification buffer and 1.56μL polymerase enzyme per well. The cells were then washed twice with buffer B for 10 min. Subsequently, in order to be able to detect EdU positive cells, the Ibidi slides were incubated with a secondary antibody solution containing mouse or rabbit Alexa Fluor 488 (ThermoFisher Scientific), depending on the used anti-biotin antibody host species. The secondary antibodies were diluted 1:1000 in buffer B with the addition of 1:2000 DAPI and incubated for 30 min at 37°C. After final washes, slides were imaged using a Leica Thunder (64x, oil) and analyzed using CellProfiler.

Comet assay

After isolation and FACS sorting of 2000-5000 cells per condition, they were imbedded in 0.8% SeaPlaque low-melting point agarose (Lonza) on 2-well comet slides (Trevigen) and lysed overnight at 4°C in lysis buffer: 2.5M NaCl, 100mM EDTA and 10mM Tris (pH10), supplemented with 10% DMSO and 1% Triton X-100.

For OGG1 comet assay, the slides were washed with PBS, and incubated with 0.08U of hOGG1 (hOGG1 FLARE Assay Kit, Trevigen) per gel in a humidified chamber for 10 min at 37°C as was previously described (Smith et al., 2006). Afterward they were processed as for normal alkaline comet assay.

For alkaline comet assays, slides were washed after overnight lysis and incubated 40 min in denaturation buffer (300 mM NaOH, 1 mM EDTA) followed by electrophoresis for 20 min at 21V and 300mA. For neutral comet assays, slides were washed and incubated for 60 min in electrophoresis buffer (300mM Sodium Acetate, 100mM Tris, pH 8.3) followed by electrophoresis for 30 min at 21V and 300mA.

Afterward, all slides were washed with PBS, fixed in ice-cold ethanol for 10 min and dried at 37°C. If cells were pulsed with EdU, slides were incubated with Click-iT Cell Reaction buffer using the Alexa Fluor 647 azide for 15 min, washed with PBS and dried at 37°C. DNA staining was done with SYBR gold (ThermoFisher Scientific) for 10 min, followed by washing with PBS and drying at 37°C. Samples were imaged using the IN Cell Analyzer 2500 HS (GE Healthcare Life Sciences) and analyzed using the Open Comet plugin for Fiji (ImageJ).

DNA fiber assay

After isolation and FACS sorting, 2000-8000 cells per condition were incubated 30 min at 37°C in serum-free StemSpan SFEM medium (STEMCELL Technologies), supplemented with 1% penicillin/streptomycin and 2% L-glutamine, to reactivate their metabolism. Subsequently 19mM 5-Chloro-2′-deoxyuridine (CldU) was added to the medium for 30 min. Medium was exchanged after short centrifugation to contain 28mM 5-iodo-2′-deoxyuridine (IdU) for 30 min. Afterward, DNA fiber spreads were produced as previously described (Mijic et al., 2017). In short 3μL of cell suspension was added to 7μL lysis buffer (200 mM Tris-HCl, pH 7.5, 50 mM EDTA, and 0.5% (w/v) SDS) on a glass slide. After 8 min, the slides were tilted at 15–45°, and the resulting DNA spreads were air dried, fixed in 3:1 methanol/acetic acid overnight at 4°C. The fibers were denatured with 2.5 M HCl for 1 h, washed with PBS and blocked with 0.2% Tween 20 in 1% BSA/PBS for 40 min. Anti-BrdU antibodies recognizing CldU (1:500, ab6326; Abcam) and IdU (1:100, B44, 347,580; BD Biosciences) were incubated for 2.5 h in the dark at room temperature (RT), followed by 1 h incubation with secondary antibodies at RT in the dark: anti–mouse Alexa Fluor 488 (1:300, Invitrogen) and anti–rat Cy3 (1:150, Jackson ImmunoResearch Laboratories, Inc.). Fibers were visualized using a Leica DMI6000 microscope (64x, oil) and analyzed using ImageJ software.

S1 nuclease fiber assay

For S1 nuclease fibers, after nucleotide incubations (as in DNA fiber assay), cells were incubated with 200μL of CSK100 buffer (100mM NaCl; 20mM HEPES; 3mM $MgCl_2$; 300mM sucrose; 0.5% Triton X-100 in water) for 5 min and subsequently washed with PBS using 5 min centrifugation at 4600*g*. Next 200μL S1 buffer (30mM Sodium Acetate pH 4.6; 10mM Zinc Acetate; 5% Glycerol; 50 mM NaCl in water and adjusted to pH 4.6) was added with or without 20 U/mL S1 nuclease (ThermoFischer Scientific) for 30 min at 37°C. Next, cells were washed with PBS again with 5 min centrifugation at 4600*g*. Finally, spreading and staining were performed as described above, except with a lysis time of 5 min.

Transcriptome analysis

After isolation and FACS sorting, RNA was extracted using the RNeasy Micro Kit (Qiagen) according to the company's instructions. Samples were treated with DNAse I on the column and collected in 12μL of RNAse-free water. Library-preparation, sequencing and data analysis were performed by the Functional Genomics Center Zurich.

Reads were quality-checked with FastQC. Sequencing adapters were removed with Trimmomatic (Bolger et al., 2014) and aligned to the reference genome and transcriptome of Mus Muscu-lus (GENCODE, GRCm38,p6) with STAR v2.7.3 (Dobin et al., 2013) using the following options:

- -outFilterType BySJout –outFilterMatchNmin 30 –outFilterMismatchNmax 10 –outFilterMismatchNoverLmax 0.05 –outMultimapperOrder Random –alignSJDBoverhangMin 1 –alignSJoverhangMin 8 –alignIntronMax 100,000 –alignMatesGapMax 100,000 –outFilterMultimapNmax 50 –chimSegmentMin 15 –chimJunctionOverhangMin 15 –chimScoreMin 15 –chimScoreSeparation 10 –outSAMstrandField intronMotif –alignEndsProtrude 3 ConcordantPair.

Distribution of the reads across genomic isoform expression was quantified using the R package GenomicRanges (Lawrence et al., 2013) from Bioconductor Version 3.10. Minimum mapping quality, as well as minimum feature overlaps, was set to 10. Multi-overlap was allowed. Differentially expressed genes were identified using the R package edgeR (Robinson et al., 2010) from Bioconductor Version 3.10, using a generalised linear model (glm) regression, a quasi-likelihood differential expression test and the trimmed means of M-values normalisation. Both GenomicRanges and edgeR analyses were performed using the SUSHI framework (Hatakeyama et al., 2016).

EM analysis

The procedure was performed as recently described (Zellweger and Lopes, 2018), with modifications described below. After RBC lysis, cells were cultured for 1 h in in serum-free StemSpan SFEM medium (STEMCELL Technologies), supplemented with 1% penicillin/streptomycin and 2% L-glutamine and with 25 nM CPT where indicated. Afterward, cells were resuspended in PBS, and cross-linked with 4,5′, 8-trimethylpsoralen (10 μgml−1 final concentration), followed by irradiation pulses with UV 365 nm monochromatic light (UV Stratalinker, 1800; Agilent Technologies). For DNA extraction, cells were lysed (1.28 M sucrose, 40 mM Tris-HCl (pH 7.5), 20mM MgCl2, and 4% Triton X-100; Qiagen) and digested (800 mM guanidine-HCl, 30 mM Tris-HCl (pH 8.0), 30mM EDTA (pH 8.0), 5% Tween 20, and 0.5% Triton X-100) at 50°C for 2 h in presence of 1 mg/mL proteinase K. The DNA was purified using chloroform/isoamylalcohol (24:1) and precipitated in 0.7 volume of isopropanol. Finally, the DNA was washed with 70% EtOH and resuspended in 200 μL Tris-EDTA (TE) buffer.

Restriction enzyme of 100 U (PvuII high fidelity, New England Biolabs) were used to digest 12 μg of DNA for 4–5 h. To purify and concentrate the DNA, an Amicon size-exclusion column was used. DNA was then resuspended in TE buffer. The benzyldimethylalkylammonium chloride method was used to spread the DNA on the water surface and then load it on carbon-coated 400-mesh copper grids. Subsequently, DNA was coated with platinum using a high vacuum evaporator MED 020 (BalTec). Microscopy was performed with a transmission electron microscope (Tecnai G2 Spirit; FEI; LaB6 filament; high tension ≤120 kV) and picture acquisition with a side mount charge-coupled device camera (2600 × 4000 pixels; Orius 1000; Gatan, Inc.). For each experimental condition, at least 70 replication fork molecules were analyzed. DigitalMicrograph version 1.83.842 (Gatan, Inc.) and ImageJ (National Institutes of Health) were used to process and analyze the images.

Primpol antibody generation

An antibody was raised in a rabbit that was immunized with recombinant protein containing amino acids 1-240 of murine primpol. To obtain the antigen the corresponding cDNA fragment of murine primpol was cloned into the pET-30 vector (Novagen), the His-tagged fusion protein expressed in *E. coli*. and purified using Ni-NTA (Qiagen) before injection. After five immunizations, serum was obtained and purified against the recombinant antigen. For that, 100–150 μg of the antigen was loaded for sodium dodecyl sulfate polyacrylamide gel electrophoresis (SDS–PAGE), transferred to a nitrocellulose membrane and stained with Ponceau S to identify the area of the membrane containing the antigen. Then, that antigen region was cut out, blocked with 2% BSA in TBS-T for 1 h and then incubated with the crude serum overnight at 4 °C. After a wash with TBS-T containing 500 mM NaCl, the antibodies that were bound to the membrane were eluted using 0.1 M glycine-HCl, pH 2.3. Finally, Tris-HCl pH 10 was added until the pH the solution containing the purified antibodies reached 7.5.

The antibody was validated using total bone marrow protein extracts from wt versus Primpol−/− mice. Briefly, 30 μg total protein from cell isolates were loaded onto 4–20% Mini-PROTEAN TGX Precast Protein Gels. Proteins were separated by electrophoresis at 16 mA followed by transferring the proteins to Immobilon-P membranes (Thermo Fisher Scientific) for 1 h at 350 mA (4°C) in transfer buffer (25 mM Tris and 192 mM glycine) containing 10% methanol. Before addition of primary antibodies (Primpol 1:1000 and H3 1:5000), membranes were blocked for 1 h in Tris-buffered saline (TBS) containing 0.1% Tween 20 and 5% milk.

Hematopoietic stem and progenitor cell counting

To determine the frequency of HSPCs in the bone marrow and the number of HSPCs per femur in mice. For each mouse 1 femur was harvested and the total bone marrow was processed into a single cell suspension. RBCs were lysed, nucleated cells were counted and the total number of cells per femur were determined. The bone marrow cells were stained with a panel of antibodies against surface receptors to distinguish HSPC populations (see isolation of hematopoietic cell subsets). Cells were analyzed by flow cytometry and at least 1.5 million single cells were recorded. Using a flow cytometry data analysis software (e.g. FlowJo), gates were set up as per standards in the field for populations of interest (POI).

Frequency of POIs were calculated as follows: (number of POI events)/(number of live single cell events). Number of POIs per femur were calculated as follows: (frequency of POI) X (number of cells counted per femur).

Competitive bone marrow transplantation assays

Total bone marrow cells were isolated from sex-matched C57BL6/J mice (CD45.1) and either PrimPol$^{+/+}$ or PrimPol$^{-/-}$ mice (CD45.2). After RBC lysis in Ammonium-Chloride-Potassium (ACK) buffer (Lonza), CD45.1 and CD45.2. bone marrow cells were mixed at a 1:1 ratio, washed, and resuspended in PBS. A total of 5 x10^{6} bone marrow cells were transferred intravenously into CD45.½C57BL/6 male and female recipient mice that had been irradiated 24 h before (two doses of 5.5 Gy separated 4 h). For the first four weeks after cell transfer, 2 mg/mL neomycin was added to the drinking water of recipient mice. Blood samples were collected and analyzed 4, 10, 16 and 29 weeks after cell transfer. At week 29, mice were euthanized, and bone marrow cells were isolated and stained for flow cytometry analysis.

Single cell suspensions were obtained from peripheral blood or bone marrow and erythrocytes were lysed in ACK buffer. Fc receptors were blocked with anti-mouse CD16/CD32 antibodies (BD Pharmingen) and cells were stained with the following fluorophore or biotin-conjugated anti-mouse antibodies: Lineage antibody cocktail (conjugated to BV421), c-Kit/CD117 (APC-H7), Sca-1 (FITC), CD34 (PE), Flk-2 (APC), SLAM/CD150 (BV785), B220 (FITC), CD3e (BV711), CD11b (V450), Ly6G/Ly6C (biotin), CD45.1 (BUV661), CD45.2 (PerCP-Cy5.5). Streptavidin (BD) was used for biotin-conjugated antibodies. Live cells were detected by DAPI, 7AAD (BD Pharmingen) or LIVE/DEAD Fixable Yellow Dead Cell Stain (Thermo Fisher) staining. Samples were acquired on LSRFortessa and analyzed with FlowJo V10.4.2 software.

QUANTIFICATION AND STATISTICAL ANALYSIS

To assess reproducibility of specific effects across biological replicates, in Figures 1B and S2A,B, Figure S3A-C,F, Figure S5B-D,F,G,I, Figure S6A,E,F, Figure S7B,D,E and Figure S8A, the average of the medians from the indicated number of biological replicates per condition was plotted as OTM, fiber track length or other.

After normality testing by Shapiro-Wilk test, samples were analyzed with GraphPad Prism using either the unpaired Welch's unequal variances t-test (Figure 1B; Figure 2G; Figure 4C; Figure S2A,B; Figure S3A-C, F; Figure S5B-D,F,G,I Figure S6A,E,F; Figure S7B,D,E; Figure S8A) or one-way ANOVA(Figure 4B; Figure S8D) for plots with combined data of replicates or Kruskal-Wallis test for individual biological replicates (Figures 1D–1H; Figure S2C-G,I; Figures 2B and 2E; Figure S5A; Figure 3C,E,F; Figure S7K).